frontiers in Ecology and Evolution

ORIGINAL RESEARCH
published: 24 May 2021
doi: 10.3389/fevo.2021.654846

Diversity in the Development of the Neuromuscular System of Nemertean Larvae (Nemertea, Spiralia)

*Jörn von Döhren**

Institute of Evolutionary Biology and Ecology, University of Bonn, Bonn, Germany

In studies on the development of nervous systems and musculature, fluorescent labeling of neuroactive substances and filamentous actin (*f-actin*) of muscle cells and the subsequent analysis with confocal laser scanning microscopy (CLSM), has led to a broad comparative data set for the majority of the clades of the superphylum Spiralia. However, a number of clades remain understudied, which results in gaps in our knowledge that drastically hamper the formulation of broad-scale hypotheses on the evolutionary developmental biology (EvoDevo) of the structures in question. Regarding comparative data on the development of the peptidergic nervous system and the musculature of species belonging to the spiralian clade Nemertea (ribbon worms), such considerable knowledge gaps are manifest. This paper presents first findings on fluorescent labeling of the FMRFamide-like component of the nervous system and contributes additional data on the muscle development in the presently still underrepresented larvae of palaeo- and hoplonemertean species. Whereas the architecture of the FMRFamide-like nervous system is comparably uniform between the studied representatives, the formation of the musculature differs considerably, exhibiting developmental modes yet undescribed for any spiralian species. The presented results fill a significant gap in the spiralian EvoDevo data set and thus allow for further elaboration of hypotheses on the ancestral pattern of the musculature and a prominent component of the nervous system in Nemertea. However, with respect to the variety observed, it is expected that the true diversity of the developmental pathways is still to be discovered when more detailed data on other nemertean species will be available.

Keywords: immuno-staining, neuromuscular system, development, heterochrony, Nemertea, Lophotrochozoa, evolution, EvoDevo

OPEN ACCESS

Edited by:
Fernando Casares, Andalusian Center for Developmental Biology (CABD), Spain

Reviewed by:
Conrad Helm, University of Göttingen, Germany
Jose Maria Martin-Duran, Queen Mary University of London, United Kingdom

***Correspondence:**
Jörn von Döhren
jdoehren@evolution.uni-bonn.de

Specialty section:
This article was submitted to Evolutionary Developmental Biology, a section of the journal Frontiers in Ecology and Evolution

Received: *17 January 2021*
Accepted: *26 March 2021*
Published: *24 May 2021*

Citation:
von Döhren J (2021) Diversity in the Development of the Neuromuscular System of Nemertean Larvae (Nemertea, Spiralia). Front. Ecol. Evol. 9:654846. doi: 10.3389/fevo.2021.654846

INTRODUCTION

Bilaterian animals are currently grouped into three major superphyla, Ecdysozoa, Deuterostomia, and Spiralia (Halanych et al., 1995; Aguinaldo et al., 1997; Giribet, 2002, 2016; Dunn et al., 2008, 2014; Hejnol et al., 2009; Edgecombe et al., 2011). Despite recent advances in metazoan systematics, there is no robustly supported phylogeny of Spiralia, with numerous, but sometimes contradicting tree topologies recently published (Laumer et al., 2015, 2019; Kocot et al., 2017; Marlétaz et al., 2019). Currently, it seems undisputed that Spiralia comprise at least Platyhelminthes (*sensu stricto*, i.e., to the exclusion of Acoelomorpha), and Lophotrochozoa that develop either via a typical trochophore-type larva or possess a

lophophore, a tentacle feeding apparatus that is supported by an inner coelomic cavity. Gnathifera is also often included in Spiralia (Laumer et al., 2015; Kocot, 2016; Marlétaz et al., 2019).

No other metazoan superphylum shows such an enormous diversity of morphologies as Spiralia and as a consequence, body wall musculature and nervous systems are also highly diverse (Wanninger, 2015). This diversity in morphologies and hence the body wall muscles and nervous systems is somewhat puzzling, since most members of Spiralia share a stereotypic, spiral cleavage (Boyer and Henry, 1998; Lambert, 2010; Nielsen, 2010; Martín-Durán and Marlétaz, 2020). It is characterized by a spiral arrangement of the blastomeres, with quartets of cells in a helicoidal arrangement above each other, that each have a determined fate in the future morphology of the species. The fates of the respective blastomeres are reported to be very conservative, even between phyla within Spiralia (Lambert, 2010; Martín-Durán and Marlétaz, 2020). Thus, highly diverse adult body plans result from a stereotypic, only marginally variable embryogenesis. The solution to this paradox may be that the majority of the morphological diversity observed in adult spiralian lineages results from diversification of post-embryonic development.

Post-embryonic development in the spiralian subclade Lophotrochozoa is characterized by a planktonic larval stage that more or less gradually develops into the benthic adult shape (Nielsen, 2004, 2005; Nezlin, 2010). During the time of larval life, the organism is subject to selection that shapes the larval morphology, but also has an impact on its metamorphosis to the adult body organization. Since the most promising approach to elucidating the evolution spiralian morphological diversity is seen to lie in investigating post-embryonic development, development of the musculature and nervous systems has recently gained much attention (Wanninger, 2009, 2015; Nezlin, 2010; Richter et al., 2015). Myo- and neurogenesis have been studied by fluorescent staining with phalloidin for muscles or antibodies against various neuroactive substances for subsets of the nervous system and examined with confocal microscopic setups. The most prominent spiralian clades Annelida and Mollusca are currently most extensively studied (Bleidorn et al., 2015; Wanninger and Wollesen, 2015). For the lophophorate taxa Brachiopoda, Ectoprocta, and Phoronida, detailed data on musculature and nervous system in the larval stages and comparison with the adult musculature has been obtained more recently (Santagata and Zimmer, 2002; Santagata, 2004, 2008a,b, 2011; Wanninger et al., 2005; Gruhl, 2008, 2009; Altenburger and Wanninger, 2009, 2010; Nielsen and Worsaae, 2010; Temereva and Wanninger, 2012; Temereva and Tsitrin, 2013, 2014).

Some smaller, indubitably spiralian taxa however, could not yet be consistently placed on the spiralian tree of life (Kocot et al., 2017; Laumer et al., 2019). Among the most notorious of these are Nemertea, that also primarily possess pelagic larvae (Maslakova and Hiebert, 2014). Nemertea (ribbon worms) is a comparably small phylum of worm-shaped, mostly marine animals comprising approximately 1300 species (Kajihara et al., 2008). As adults, the majority of nemertean species are photophobic predators that capture their prey with an eversible, muscular proboscis that is housed in a secondary body cavity, called rhynchocoel. Based on molecular data, three major lineages are currently recognized: Hoplonemertea, Pilidiophora, and Palaeonemertea (Andrade et al., 2012, 2014; Kvist et al., 2014). Hoplonemertea possess a proboscis that is armed with a stylet apparatus consisting of one or multiple calcareous stylets, employed to stab the prey and poison it with a species-specific cocktail of toxic substances (McDermott and Roe, 1985; Chernyshev, 2000; von Reumont et al., 2020). Pilidiophora are characterized by a specific type of larva, the pilidium (Thollesson and Norenburg, 2003; Maslakova, 2010a; Maslakova and Hiebert, 2014). Palaeonemertea, although characterized as monophyletic in the most recent phylogenetic analyses based on genome-scale datasets (Andrade et al., 2014), do not share any unambiguously derived morphological characters. Development in the palaeo- and hoplonemertean species has traditionally been described as "direct," since no explicitly larval characters had been detected (Iwata, 1960; Maslakova, 2010a; Maslakova and Hiebert, 2014). More recently however, the pelagic developmental stage of Hoplonemertea has been characterized as decidula larva, due to a transitory larval epidermis found in many representatives of this clade (Maslakova and von Döhren, 2009; Hiebert et al., 2010; Maslakova, 2010a; Maslakova and Hiebert, 2014). The ancestral larval type of Palaeonemertea has been postulated to represent a so-called hidden trochophore larva (Maslakova et al., 2004).

With respect to development of nervous system and musculature, nemertean larvae are clearly understudied. Information on the development of the nervous system of Nemertea by means of fluorescent antibody labeling and confocal microscopy is almost exclusively restricted to the serotonin immunoreactive component in about a handful of mostly pilidiophoran species and the development of the body wall musculature by fluorescent labeling with phalloidin has never been in the focus of any comparative investigation (Hay-Schmidt, 1990; Martindale and Henry, 1995; Maslakova et al., 2004; Schwartz, 2009; Chernyshev and Magarlamov, 2010; Hiebert et al., 2010; Maslakova, 2010b; von Döhren, 2011, 2015, 2016; Chernyshev et al., 2013; Hindinger et al., 2013; Beckers and von Döhren, 2015; Hiebert and Maslakova, 2015a,b; Martín-Durán et al., 2015). This study aims at a comparative description of the development of the body wall musculature and of the FMRFamide immunoreactive component, a subset of the peptidergic nervous system in several non-pilidiophoran representatives that possess the type of development that has traditionally been termed as "direct." Both hoplo- and palaeonemertean representatives were investigated. The results obtained are expected to provide additional data to trace the evolution of morphological diversity within the highly diverse superphylum Spiralia.

MATERIALS AND METHODS

Species and Collection Sites

Adult, sexually mature specimens of both sexes of *Tubulanus polymorphus* Renier, 1804 (Tubulanidae, Palaeonemertea) were collected in the intertidal zone close to the Station Biologique de Roscoff, France in July and August 2014. The animals are endobenthic and had to be dug out of the sand. After collection, the specimens were kept in running seawater at the Station. Sexually mature adult males and females of *Carinoma*

armandi (McIntosh, 1875) (Carinomidae, Palaeonemertea) were obtained by digging in the intertidal sandflat of the Anse de Pouldohan near Concarneau, France in June 2018. Animals were subsequently transported to the Institute of Evolutionary Biology and Ecology of the University of Bonn (IEZ), were they were kept in plastic aquaria filled with seawater and sand from the collection site with weakly water changes. *Carinoma mutabilis* Griffin, 1898 (Carinomidae, Palaeonemertea) males and females were found sexually mature from January to February, 2007 in the intertidal sandflat of False Bay on San Juan Island, WA, United States. They were taken to Friday Harbor Laboratories where they were kept in running seawater. *Carcinonemertes carcinophila* (Kölliker, 1845) (Monostilifera, Hoplonemertea) is ectoparasitic on the decapod crab *Carcinus maenas* (Linnaeus, 1758). The crabs were collected during cruises with the research vessel Mya in the vicinity of the AWI Wattenmeerstation in List auf Sylt, Germany in June 2012. At the AWI Wattenmeerstation, gravid *C. maenas* females were inspected for sexually mature male and female *C. carcinophila* individuals that were removed from between the egg masses of the crabs. The nemerteans were kept at 8°C in natural sea water until they were transported to the IEZ, were they were kept in large plastic petri dishes at comparable temperatures. *Amphiporus* sp. (Monostilifera, Hoplonemertea) is a yet undescribed free-living, benthic nemertean species. A formal description of this species is planned for the near future. One sexually mature female and two males were found under stones submerged in approximately 0.5 m deep water on the coast of Giglio island, Italy in June 2013. Animals were transported to the IEZ were they were kept at 18 °C in plastic aquaria with artificial sea water and medium sized stones to provide shelter from light.

Obtaining and Rearing Larvae

Larvae of palaeonemetean species were obtained by artificial fertilization from dissected oocytes that were fertilized with a diluted suspension of sperm dissected from the males. Prior to fertilization, the oocytes were placed in sterile-filtered natural seawater from the respective collection site until they round up, which is usually accomplished within 20–30 min. Zygotes were kept in sterile filtered sea water from the collection site of their parents. In the hoplonemertean species, eggs could not be artificially fertilized. In *C. carcinophila*, the eggs are shed into parchment-like gelatinous tubes. The egg strings are normally found, wrapped around the pleopods between the developing eggs of the host crab, but *C. carcinophila* females in petri dishes laid eggs after warming up the water to 18°C. In *Amphiporus* sp. the eggs were shed at night-time and were transferred to clean seawater the next morning. The containers with the larvae of *T. polymorphus* and *C. mutabilis* were cooled by placing them up to half of their height in running seawater (*T. polymorphus* 14–16°C, *C. mutabilis* at 8–10°C). Larvae of *C. armandi* were kept at 12°C, those of *C. carcinophila* and *Amphiporus* sp. at 18°C. Clean filtered seawater was replaced every 2–3 days. Although several food items were offered, e.g., quartered sea urchin embryos (to *C. mutabilis*), blue mussel oocytes (to *C. armandi*), and brine shrimp nauplii (to *Amphiporus* sp.), none of the larvae were observed to feed.

Sampling and Fixation of Larvae

The larvae were fixed at different times after fertilization (*C. mutabilis*: 1–2, 3, and 5 days; *C. armandi*: 1–3, 5, and 7 days; *T. polymorphus*: 1–4, 6, and 9 days) or egg-deposition (*C. carcinophila*: 3 and 4 days; *Amphiporus* sp.: 1–5, 7, 10, 14, and 18 days). To prevent possible muscle contraction during fixation, hatched larvae that show muscular contraction (usually from 3 days after fertilization or egg-deposition) were relaxed in a 1:1 mixture of sterile-filtered seawater and aqueous $MgCl_2$ solution of 0.33 mol l^{-1} (*C. mutabilis*) or 0.37 mol l^{-1} (remaining species) at room temperature until no muscle contractions were observed (usually after 10–15 min). Specimens were fixed in 4% (v/v) formaldehyde (prepared from 1 part of a 16% aqueous paraformaldehyde solution, EMS or VWR Chemicals, mixed with 3 parts of sterile-filtered sea water) at 18°C or at room temperature for 30 min. After fixation, larvae were washed three times for 10 min each in 0.1 M phosphate buffer saline (PBS, pH 7.4; Fisher Scientific for *C. mutabilis*, own formulation for the other species) at 18°C or at room temperature. Except for *C. mutabilis*, larvae were stored at 4–8°C in the same buffer but with 0.01% (w/v) NaN_3 (Roth) added to prevent microbial growth. In the larvae of the former species, no NaN_3 was added to the buffer for storage.

Immunohistochemistry and Fluorescent Labeling

Up to 12 larvae of *C. mutabilis* were blocked in 6% normal donkey serum (Jackson Immunoresearch) in PBS with 0.1% Triton X-100 (Fisher Scientific), hereafter referred to as 0.1% PBT for 2 h at room temperature. After washing with 5 changes of 0.1% PBT for 5 min each, larvae were incubated in rabbit-anti-FMRFamide (Immunostar) at 1:500 dilution in PBS overnight at 4°C followed by washing with three changes of 0.1% PBT for 10 min each at room temperature. Subsequently, the specimens were incubated in donkey-anti-rabbit antibody conjugated with Alexa Fluor 488 (Molecular Probes) at a dilution of 1:600 for 2 h at room temperature and afterward rinsed with three changes of PBS, each for 10 min. For immunostaining in the remaining species, depending on the size between 10 and 15 specimens were permeabilized in three changes of PBS with 0.3% Triton X-1000 (0.3% PBT) each for 10 min at room temperature. Subsequently, specimens were blocked in 10% normal goat serum (NGS, Sigma-Aldrich) in 0.3% PBT for 2 h at room temperature and afterward incubated with the primary antibodies overnight at 18°C. Antibodies used were against FMRFamide produced in rabbit (Abcam) at a dilution of 1:1000 and against acetylated α-tubulin raised in mouse (Sigma-Aldrich) at a dilution of 1:200 in 0.3% PBT with 10% NGS. In double labeling experiments, both antibodies were applied simultaneously. After incubation with primary antibodies, specimens were washed in three changes of 0.3% PBT for 10 min each at room temperature. As secondary antibodies, goat-anti-rabbit conjugated with Alexa Fluor 488, Alexa Fluor 568 or Alexa Fluor 633 and goat-anti-mouse, conjugated with Alexa Fluor 488 or Alexa Fluor 633 (Invitrogen) were used at a concentration of 1:100 to 1:400 in 0.1% PBT with 10% NGS. The specimens were incubated with the secondary antibodies for 2 h at room temperature and

subsequently washed 3 times for 10 min each in 0.1% PBT. In double labeling experiments, both antibodies, against mouse and against rabbit with different conjugated fluorophores, were applied simultaneously.

For labeling of filamentous actin (*f-actin*), larvae of *C. mutabilis* were permeabilized in three changes of PBT (10 min each), and stained with Bodipy FL phallacidin (Molecular Probes) at a dilution of 1:100 for 40 min at room temperature. After staining, larvae were rinsed three times with PBS for 10 min each. In the remaining species f-actin was labeled with phalloidin coupled to Alexa Fluor 488 or tetramethylrhodamine-isothiocyanate (TRITC) (Invitrogen) at a dilution ranging from 1:100 to 1:200 for 40 min up to 2 h. In double labeling experiments with immunostainings, phalloidin was added together with the secondary antibodies. After staining, larvae were rinsed three times each for 10 min in PBS (*C. mutabilis* larvae) or 0.1% PBT (larvae of remaining species).

Mounting, Confocal Laser Scanning Microscopy and Image Processing

All samples were mounted on coverslips coated with poly-L-lysine (Sigma-Aldrich). Larvae of *C. mutabilis* stained with antibodies against FMRFamide were mounted in Vectashield (Vector Laboratories). All larval stages of *C. carcinophila* were mounted in 90% (v/v) glycerol in PBS. The remaining larvae were quickly dehydrated in isopropanol (1 min each in 70, 85, and 95%, 2 times 100%), cleared in three changes of BABB (mixture of 1 part of benzyl alcohol and 2 parts of benzyl benzoate) for 10 min each, mounted in BABB on glass slides with several layers of 100-μm-thick adhesive tape or clay pieces as spacers, and sealed with nail polish.

To examine *C. mutabilis*, a Bio-Rad Radiance 2000 laser scanning confocal system mounted on a Nikon Eclipse E800 microscope with a 40 × 1.3 NA oil immersion objective and an excitation wavelength of λ = 488 nm (light blue) was used. Optical section thickness was set to 1 μm and images were recorded at 8-bit image depth at a resolution of 1024 × 1024 pixels. For signal detection in the remaining species a Leica TCS/SPE confocal laser scanning system mounted on a Leica DM 2500 microscope was used. Alexa Fluor 488 was excited with the 488 nm-, Alexa Fluor 568 and TRITC with the 532 nm- (green), and Alexa Fluor 633 with the 635 nm-laser line (red). All images were recorded with a 40 × 0.75 NA dry objective. For double-stained specimens the sequential excitation/detection setting was used. Stacks of images were recorded with an optical section thickness of 0.88 μm with a resolution of 1024 × 1024 pixels and an image depth of 8 bit.

Image stacks were processed with the Fiji distribution package of ImageJ by W. S. Rasband, NIH, version 1.53c (Schindelin et al., 2012; Schneider et al., 2012). To produce two dimensional images from the recorded stacks, the maximum-intensity stack-projection function was used. Images were subsequently adjusted using global contrast settings, gamma function (detailed in the figure subheadings), unsharp mask-, and remove outlier-filters. Resulting images were rotated, translated, and cropped (details of image enhancement are listed in **Supplementary Table 1**). Mounting and annotation of images and line drawings were made with Adobe Illustrator CS6. **Supplementary Videos** were produced in Fiji/ImageJ version 1.53c. The respective image series were rotated in the x- and y-axes (so that the apical pole/frontal end is oriented up in every video) and cropped using the respective commands. The image series were subjected to background subtraction (command "Subtract Background..." at default settings), global contrast adjustment (command "Enhance Contrast...", saturated pixels: 0.3% and "use stack histogram" checked, followed by command "Adjust Brightness/Contrast" with lower cut-off level set to 2), and noise reduction (command "Remove Outliers..." at default settings). After annotation of the image series the images were saved as avi-files with JPEG-compression at a frame rate of 4 *fps* (frames per second).

RESULTS

Tubulanus polymorphus (Tubulanidae, Palaeonemertea)

Post-embryonic Development

At 14–16°C, hatching in *T. polymorphus* takes place before 1 day after fertilization (*1-dpf*), resulting in spherical free-swimming developmental stages. In the majority of specimens observed, gastrulation is completed after 1 day of development and the epidermal cells are adorned with a dense coat of epidermal cilia visualized by acetylated α-tubulin-like immunoreactivity (**Figure 1A**: α-*tub-lir* at 2-dpf). The blastopore has begun to shift its position from opposite of the apical tuft to a more anterior location as it becomes the mouth opening and foregut at 2-dpf (**Figure 1A**: *fg*). The translocation of the mouth opening to more anterior continues through all observed stages; a closure of the blastopore is not observed. Additionally, at 1-dpf, an apical pit with a tuft of elongated cilia and pair of apical epidermal invaginations, each on either side of the apical pit are forming (**Figure 1A**: *at* at 2-dpf). The cilia of the apical tuft elongate to attain their maximal length at 3-dpf. The epithelium of the midgut becomes ciliated between 1- and 2-dpf and the first signals of ciliated nephridia also appear at that time (**Figure 1A**: *mg* and *pn*). In the course of further development, the larvae become more elongate and ellipsoid. General internal anatomy remains largely unchanged until 9-dpf, the oldest examined stage (**Figure 2B**). Neither the formation of the anal opening, nor the formation of a proboscis rudiment is observed until the end of the examined development. The larva of *T. polymorphus* does not possess eyes in any of the observed stages.

FMRFamide-Like Immunoreactivity

In post-gastrula stages of *T. polymorphus*, there are several more or less spherical signals of comparable size (300–400 nm in diameter) distributed over the surface of the larva. Most of the signals are located at the level of the epidermal cells, but do not reach their surface. Others are clearly superficial. No clear neurite-like signals could be observed at this time of development. The epidermis shows small, spot-like signals all over its surface, without any conspicuous aggregations detectable (**Figure 1B** at 2-dpf). These spot-like signals are very likely unspecific staining. The first distinctive FMRFamide-like immunoreactive (*RFa-lir*) signals are observable after 1-dpf. Inside the larva, there are no strong signals, although two cell-like signals, slightly dorso-lateral underneath the apical pit show

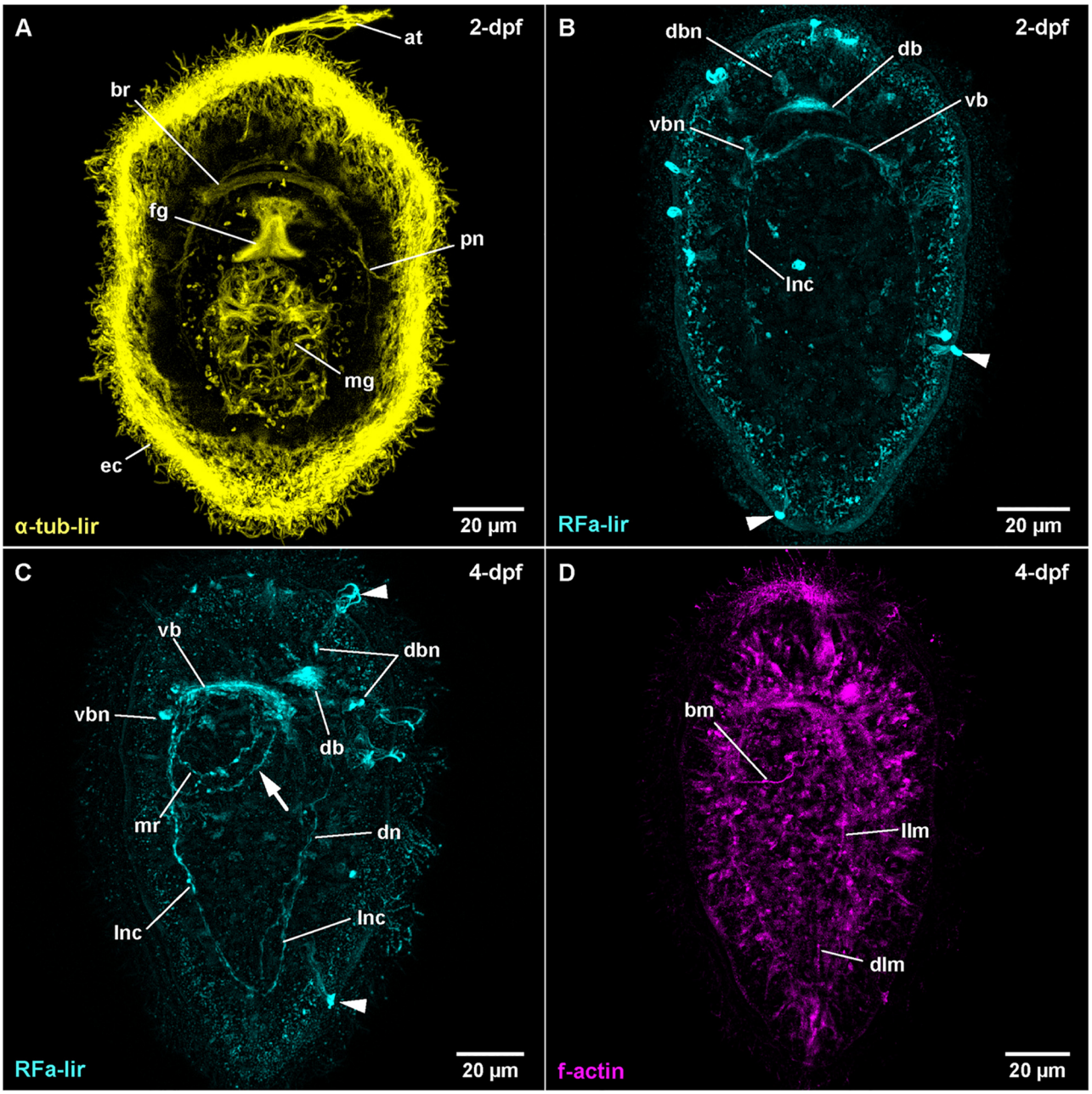

FIGURE 1 | *Tubulanus polymorphus*, (frontal is up in all images, age of larval stages indicated in top right-hand corner, dpf: days post artificial fertilization). **(A)** (γ = 0.6); projection of 31 optical sections, ventral view. **(B)** (γ = 0.8); maximum projection of 28 optical sections, dorsal view. *Arrowheads* indicate unspecific staining of epidermal gland cells. **(C)** (γ = 0.75); maximum projection of 27 optical sections, ventro-lateral view. *Arrowheads* indicate unspecific staining of epidermal gland cells, *arrow* indicates second mouth ring neurite. **(D)** (γ = 1.2); maximum projection of 14 optical sections, ventro-lateral view. at: apical tuft, bm: buccal muscle, br: brain ring, db: dorsal part of brain ring, dbn: neuron of dorsal part of brain, dlm: dorsal longitudinal muscle, dn: dorsal nerve, ec: epidermal cilia, fg: foregut, llm: lateral longitudinal muscle, lnc: lateral nerve cord, mg: midgut, mr: mouth ring neurite, pn: protonephridium, vb: ventral part of brain ring, vbn: neuron of ventral part of brain.

up slightly brighter than their surroundings. The signals seem to project distally to the apical pit and proximally seem to converge to a single signal that is oriented perpendicular to the longitudinal body axis and located slightly dorsal and anterior of the archenteron. Since this signal is in the position where the dorsal part of the brain ring is expected to form, it is interpreted as the rudiment of the dorsal part of the brain ring (**Figure 1B**: *db* at 2-dpf).

At 2-dpf, the epidermis cells still show the dot-shaped, presumably unspecific signals (**Figures 1B,C**). Inside the larva,

the neurite-like RFa-lir signals of the developing brain ring are visible (**Figure 1B**: *db* and *vb*). The strongest signals are located in the dorso-median position anterior of the developing gut, whereas the ventral brain ring is represented by a single RFa-lir neurite-like signal. On the dorsal side, there are up to 1–2 pairs of roughly spherical, dorso-laterally located and 1 medially located RFa-lir neuron-like signals (**Figure 1B**: *dbn*). Ventrally, 1–2 pairs of spherical lateral and up to three fusiform median neuron-like signals are observable in the vicinity of the brain ring neurite-like signal (**Figure 1B**: *vbn*). A bundle of few RFa-lir neurite-like signals extend from the ventral part of the brain ring bilaterally to the posterior end of the larva. These signals represent the developing lateral nerve cords (**Figure 1B**: *lnc*). Additionally, there are bright, superficial signals of a diameter of 300–400 nm observable in the epidermis, that are unevenly distributed over the entire length and circumference of the larva (**Figure 1B**: *arrowheads*). This type of signals is seen in all subsequent larval stages of *T. polymorphus* that have been investigated (**Figures 1C**, **2A**: *arrowheads*). These signals are connected to underlying, less bright fibril-like signals that fan out into the epidermis and extend through its complete width. At the level of the base of the surrounding epidermis cells, the fibril-like signals converge and thus attain a roughly pyriform, basket-like appearance. In some of these structures, similar fibril-like extensions are seen to fan out above the epidermis to the exterior (**Figure 1C**: *arrowheads* at 4-dpf). These structures are without any detectable contact to any internal, neurite-like signals observable inside the larva. Due to their similar internal and external fibrillar sub-structures, their uneven distribution and the lack of contact to the nervous system, these signals are interpreted as epidermal mucus gland cells showing unspecific staining that have partly extruded their contents in a fibrillar shape during fixation of the larvae.

During further development, the majority of developing RFa-lir nervous system-like structures have only slightly increasing in intensity. Posterior of the brain ring and between the signals of the lateral nerve cords on the ventral side of the larva, a bundle of neurites is detected to surround the mouth opening (**Figure 1C**: *mr*). The posterior semi-circle of this mouth ring neurite-bundle shows a plexus-like arrangement of its neurite-like signals. Whereas the plexus-like arrangement of the posterior semi-circle of the mouth ring neurite bundle has largely disappeared at 4-dpf, a second neurite-like signal is seen next to the posterior semi-circle of the mouth ring (**Figure 1D**: *arrow*). After 4-dpf, dorso-laterally, slightly posterior of the brain ring, 1–2 pairs of additional slightly lobate RFa-lir neuron-like signals have appeared during subsequent development (**Figure 2A**: *dbn* at 6-dpf). The dorso-lateral RFa-lir neuron-like signals posterior of the brain ring show neurite-like signals that extend from the perikarya anteriorly to the median aggregation of RFa-lir neurite-like signals of the dorsal part of the brain ring (**Supplementary File 1**). Also on the dorsal side of the larva, the first RFa-lir neurite-like signal of the longitudinally oriented dorsal nerve is forming (**Figures 1C**, **3A**: *dn*). In presumably less advanced specimens, the neurite-like signal is without connection to the dorsal part of the brain ring, whereas a connection of the

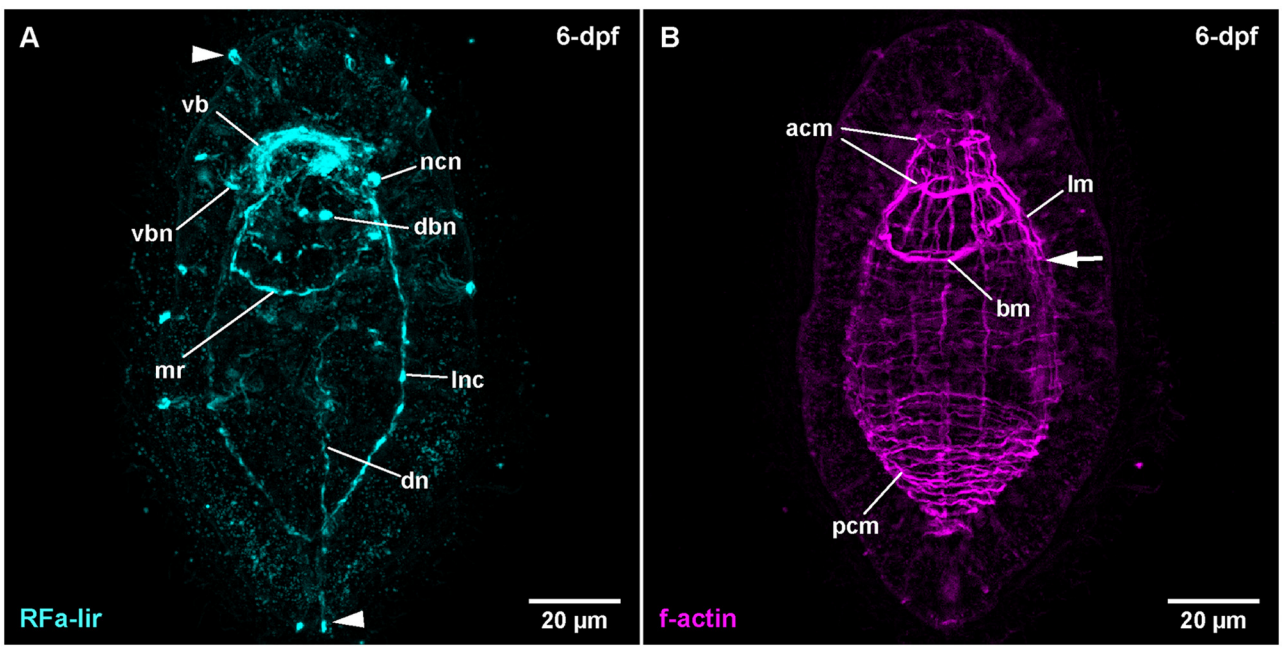

FIGURE 2 | *Tubulanus polymorphus*, (frontal is up in all images, age of larval stages indicated in top right-hand corner, dpf: days post artificial fertilization). **(A)** (γ = 0.85); maximum projection of 26 optical sections, ventro-lateral view. *Arrowheads* indicate unspecific staining of epidermal gland cells. **(B)** (γ = 0.75); same as A. *Arrow* indicates extension of lateral longitudinal muscles. acm: anterior circular muscle, bm: buccal muscle, dbn: neuron of dorsal part of brain, dn: dorsal nerve, lm: longitudinal muscle, lnc: lateral nerve cord, mr: mouth ring neurite, ncn: nerve cord neuron, pcm: posterior circular muscle, vb: ventral part of brain ring, vbn: neuron of ventral part of brain.

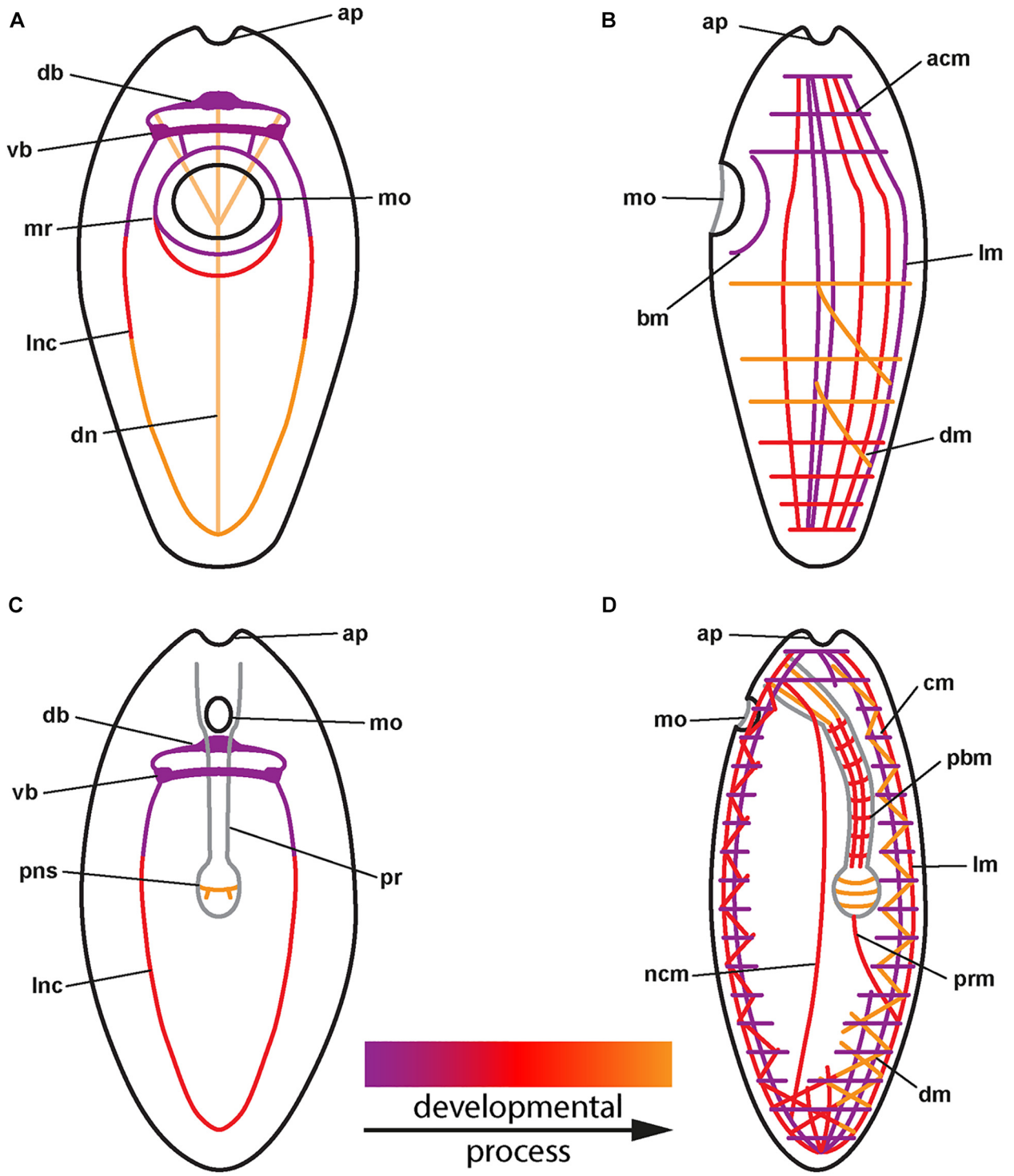

FIGURE 3 | (A) Generalized development of the nervous system in palaeonemertean species (for clarity, only neurites of main components shown). **(B)** Generalized development of the musculature in palaeonemertean species. **(C)** Generalized development of the nervous system in monostiliferan, hoplonemertean species (for clarity, only neurites of main components shown). **(D)** Generalized development of the musculature in monostiliferan, hoplonemertean species (part of the body wall muscles omitted to show internal muscular elements of proboscis and nerve cords). acm: anterior circular muscle, ap: apical pit, bm: buccal muscle, cm: circular muscle, db: dorsal part of brain ring, dm: diagonal muscle, dn: dorsal nerve, lm: longitudinal muscle, lnc: lateral nerve cord, mo: mouth opening, mr: mouth ring neurite, ncm: nerve cord muscle, pbm: proboscis muscle, pns: proboscis nervous-like signal, pr: proboscis, prm: proboscis retractor muscle, vb: ventral part of brain ring.

anterior end of the dorsal nerve neurite-like signals to the median aggregation of dorsal neurite-like signals of the brain ring is visible in presumably more advanced stages (**Figure 3A**: *dn*). Additionally, the more posteriorly located pair of dorso-lateral neuron-like signals of the brain is connected to the dorsal nerve neurite-like signal via an RFa-lir neurite-like signal that is diagonally extending from each side toward the dorsal nerve signal (**Figure 3A**–neurons not shown). Furthermore, there are up to three smaller dorso-median RFa-lir neuron-like signals detected anterior of the brain ring (**Supplementary File 1**). On the ventral side of the larva, two pairs of RFa-lir neuron-like signals have appeared in the vicinity of the brain ring and the lateral nerve cord neurite-like signals. One of them is located at the transition of the brain ring to the lateral nerve cords, the other slightly more posterior, laterally of the lateral nerve cords (**Figure 2A**: *ncn*). Posterior of the dorsal brain ring neurite-like signals, a 3rd pair of weak, dorsolateral RFa-lir neuron-like signals that is similar in shape as the existing two pairs has developed at 6-dpf (**Figure 2A**: *dbn*–only one pair visible). Anterior of the brain ring signals, on both the dorsal and the ventral side, some slender RFa-lir neuron-like signals extend in a longitudinal orientation to the anterior end of the larva. Some of the dorsally located signals are connected to the dorsal brain ring signal aggregation by forked, RFa-lir neurite-like signals, especially to the dorso-median neurite-like signal aggregation (**Supplementary File 2**). The anterior neuron-like signals are interpreted as sensory cells, their connecting neurite-like signals as the first signals of the cephalic nerves. In the oldest investigated stages (9-dpf) the dorso-median RFa-lir neuron-like signals anterior of the brain amount to up to 5, the lateral-most pair showing branching RFa-lir neurite-like signals extending from each neuron-like signal to the surface of the epidermis (data not shown).

F-Actin Labeling of Musculature

The first observable signals of muscular f-actin are observed in 4-dpf larvae. At first a single short, longitudinally oriented fiber-shaped signal is visible on the dorsal side, on the level of the mouth opening. In presumably more advanced stages of that age this first signal has elongated toward the posterior end and additional shorter longitudinally oriented signals are seen on the dorso-lateral sides of the larva, extending posterior of the mouth opening (**Figure 1D**: *dlm* and *llm*). A muscular f-actin signal running alongside the posterior rim of the mouth opening becomes apparent (**Figure 1D**: *bm*). In the same specimens, the first f-actin signals of circular muscles are formed anterior of the mouth opening and distal to the longitudinal signals (not visible in **Figure 1D**, but see **Figure 2B**: *acm* at 6-dpf).

In some more advanced specimens, the longitudinal, lateral f-actin strands extend further to the posterior end of the body and additional circular muscular f-actin signals are visible in the posterior region of the larva. By 6-dpf, more dorso-lateral longitudinal f-actin signals are seen extending along the entire length of the larva (**Figure 2B**). Additional longitudinally oriented f-actin signals are located laterally and ventro-laterally. These strands only reach to the posterior rim of the mouth opening (**Figure 2B**: *arrow*). Circular muscle signals have become more numerous, but especially in the group of signals posterior of the mouth opening, the signals are weaker anteriorly (**Figure 2B**: *pcm*). The ring-shaped signal surrounding the mouth opening is completely closed (**Figure 2B**: *bm*). During further development up to 9-dpf larvae, longitudinal signals become more numerous and seemingly more pronounced but remain confined to the dorsal, and lateral faces of the body where they are evenly spaced (**Figure 3B**). The f-actin signals of the posterior circular muscles increase in number toward the posterior end, while some of the more anteriorly located signals of this group become connected on the ventral side (data not shown).

Carinoma armandi and *Carinoma mutabilis* (Carinomidae, Palaeonemertea)

Post-embryonic Development

The water temperature during development in *C. armandi* was 12°C, whereas in *C. mutabilis*, it was in the range of 8–10°C. At 1-dpf, developmental stages of both species have hatched. In *C. armandi*, the epidermis becomes ciliated, indicated by α-tub-lir at 1-dpf. At 2-dpf, in both species an apical pit and a pair of apical invaginations are formed, one on each side of the apical pit (**Figures 4B,D**: *ap* and *li*). In *C. armandi*, the apical invaginations form slightly earlier than the apical pit. In *C. armandi*, gastrulation is completed at 2-dpf, in *C. mutabilis* at 3-dpf (**Figure 4C**). Closure of the blastopore could not be ascertained but a mouth opening if present, is not ciliated and inconspicuous. A ciliated foregut, located roughly halfway along the length of the larva, has formed in *C. armandi* at 3-dpf although it does not seem to be open to the exterior (**Figure 4D**: *fg*). The cilia of the midgut epithelium start forming at 2-dpf and become conspicuous at 3-dpf (**Figure 4D**: *mg*). In both *Carinoma* species, the lateral apical invaginations have disappeared at 5-dpf (**Figures 5A,B**). Paired, unbranched protonephridia, located one on each side of the mouth opening are detectable at 7-dpf (**Figure 5C**: *pn*). In neither of the *Carinoma* species a caudal tuft, nor the formation of the anal opening or development of the proboscis was seen during the observed period of development.

FMRFamide-Like Immunoreactivity

The earliest stage of *C. armandi*, in which internal RFa-lir signals are detectable is 2-dpf. Although, the signals observed are not stronger than the coarsely granular signals observed in the outermost layer of the large epidermis cells, the internal signals are visible against the weak autofluorescence of their surroundings (**Supplementary File 3**). Since a mouth opening is not evident in the earlier stages, it is impossible to identify whether the signals are dorsally, ventrally or laterally located. In most specimens, up to two, rarely three anteriorly located signals are detected. The signals have an elongated, sometimes pyriform outline extending from the interior with the slender part to the surface of the apical pole of the larva. The proximal portions of the signals are usually stronger. In larvae at 3-dpf, the number of signals observed in each specimen has increased to 3–6, the range indicating a sequence of appearance and subsequent

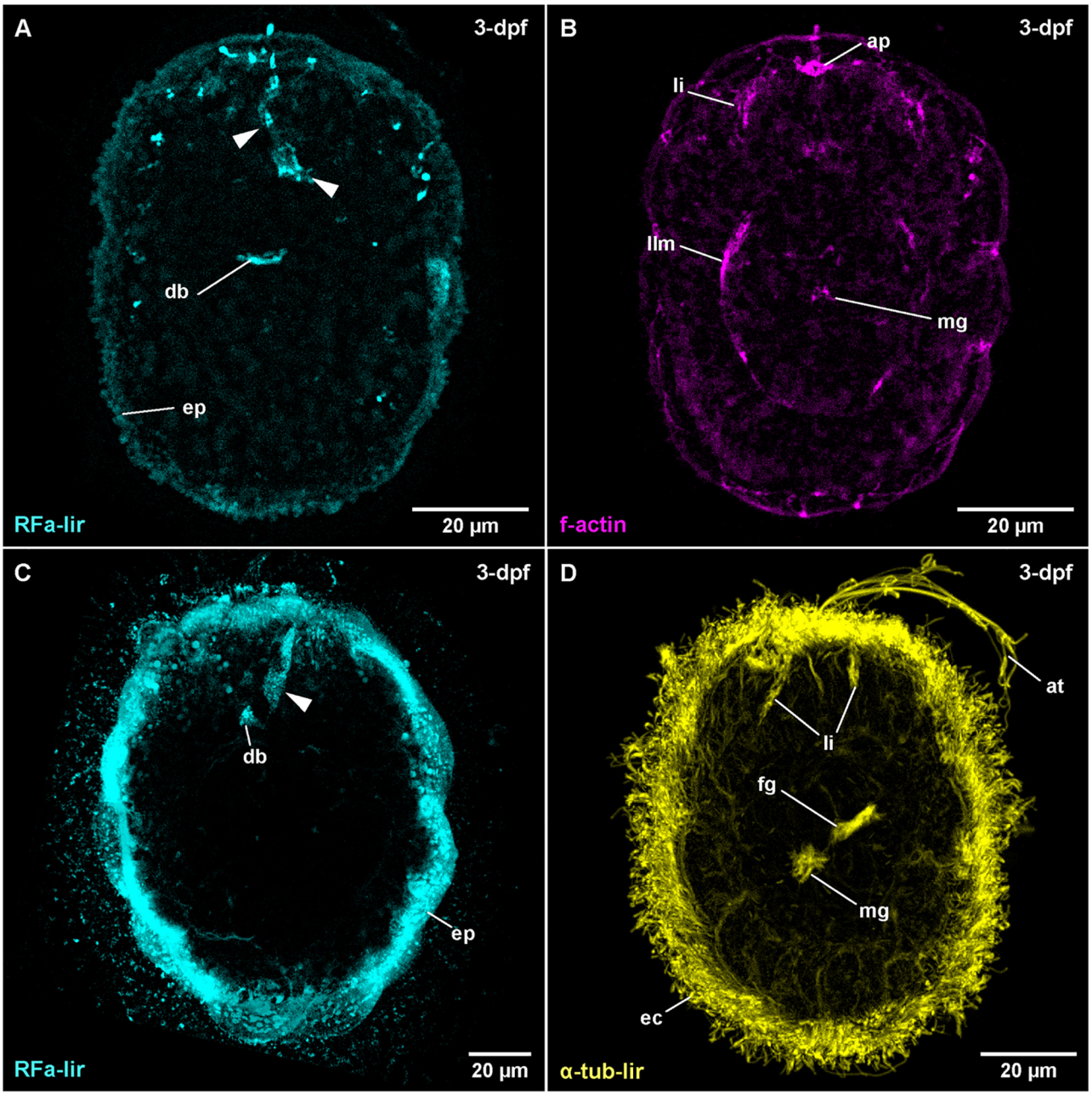

FIGURE 4 | *Carinoma* species (frontal is up in all images, age of larval stages indicated in top right-hand corner, dpf: days post artificial fertilization). **(A)** *C. armandi* (γ = 1.1); maximum projection of 11 optical sections, dorsal view. *Arrowheads* indicate different portions of transitory flask-shaped apical neuron. **(B)** *C. armandi* (γ = 1.1); same as panel **(A)** *C. mutabilis* (γ = 0.85); maximum projection of 13 optical sections, dorsal view. *Arrowheads* indicate basal portions of transitory flask-shaped apical neuron. **(D)** *C. armandi* (γ = 0.8); maximum projection of 16 optical sections, ventro-lateral view. ap: apical pit, at: apical tuft, db: dorsal part of brain ring, ec: epidermal cilia, ep: epidermis, fg: foregut, li: lateral epidermal invaginations, llm: lateral longitudinal muscle, mg: midgut.

disappearance (**Figure 4A**: *arrowheads* at 3-dpf). Interiorly, the signals usually converge on a slightly elongated signal that is oriented perpendicular to the longitudinal axis of the larva. This signal is interpreted as the first RFa-lir signal of the developing dorsal part of the brain ring (**Figure 4A**: *db*). Since by this time, the apical pit and an anterior epidermal invagination bilaterally on each side of the pit have formed, the position of the pyriform or elongated early RFa-lir signals can now be identified more precisely. The majority of signals extends from the apical pole of the larva in the vicinity of the lateral epidermal invagination or from the dorsal face between them to the dorsal brain ring rudiment, but it cannot be ruled out that few signals observed are located ventro-laterally. In *C. mutabilis* larvae at 3-dpf, up to two inconspicuous RFa-lir, fusiform, neuron-like signals are visible

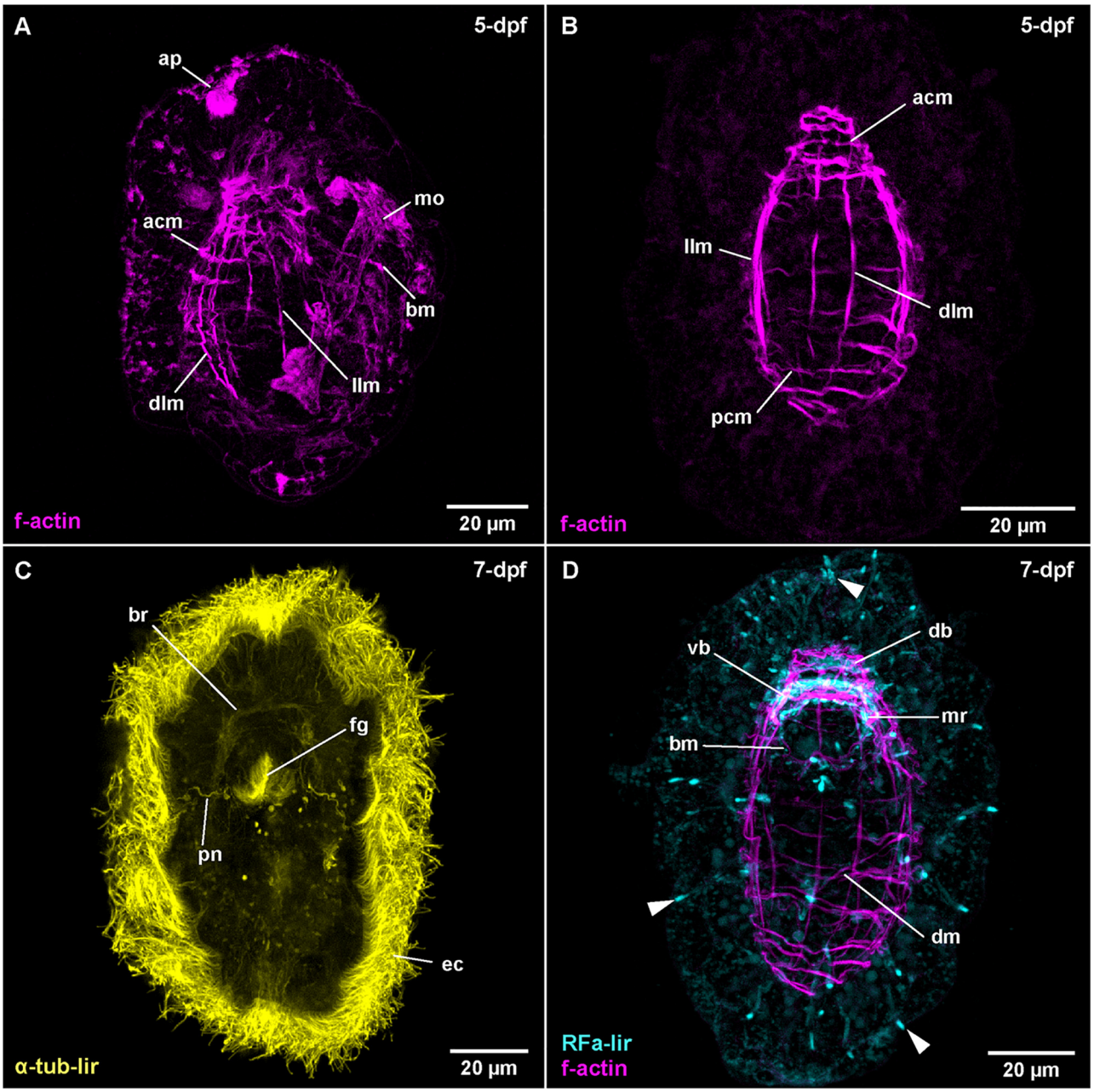

FIGURE 5 | *Carinoma* species (frontal is up in all images, age of larval stages indicated in top right-hand corner, dpf: days post artificial fertilization). **(A)** *C. mutabilis* ($\gamma = 0.9$); maximum projection of 67 optical sections, lateral view. **(B)** *C. armandi* ($\gamma = 0.8$); maximum projection of 10 optical sections, dorsal view. **(C)** *C. armandi* ($\gamma = 0.7$); maximum projection of 9 optical sections, ventral view. **(D)** *C. armandi* (RFa-lir: $\gamma = 0.7$, f-actin: $\gamma = 0.7$); maximum projection of 27 optical sections, ventral view. *Arrowheads* indicate peripheral neuron-like signals. acm: apical circular muscle, ap: apical pit, bm: buccal muscle, br: brain ring, db: dorsal part of brain ring, dlm: dorsal longitudinal muscle, dm: diagonal muscle, ec: epidermal cilia, fg: foregut, llm: lateral longitudinal muscle, mo: mouth opening, mr: mouth ring neurite, pcm: posterior circular muscle, pn: protonephridium, vb: ventral part of brain ring.

underneath the apical pole of the larva (**Figure 4C**: *arrowhead*). They converge to a third signal that is shaped like a flat cone with its tip directed apically, likely corresponding to the first rudiment of the dorsal part of the brain ring (**Figure 4C**: *db*). Thus, the observed signals are very similar to the signals observed in *C. armandi* at 2-dpf.

By 5-dpf in larvae of *C. armandi*, no pyriform apical neurons comparable to those seen in earlier stages are detectable (**Figure 5D** at 7-dpf). The RFa-lir neurite-like signals of the brain ring are now seen to form a complete ring, although the signals in the dorsal part are stronger (**Figures 3A**, **5D**: *vb* and *db* at 7-dpf). In the dorsal part there are 1 pair of dorso-lateral

and 1 median RFa-lir neuron-like signals visible, connecting to the brain ring neurite-like signals (**Supplementary File 4**). The median neuron projects a slender process into the apical pit. In the ventral part of the brain ring, there seems to be one median RFa-lir neuron-like signal connected to the brain ring neurite-like signals in some specimens (data not shown). Slightly behind the brain ring on the ventral side of the larva, a semicircle of an RFa-lir neurite-like signal anterior to the mouth opening is seen that is later completed by a posterior, albeit much weaker signal. These signals are interpreted as mouth ring neurites (**Figures 3A**, **5D**: *mr* at 7-dpf). In more elongated and therefore presumably more advanced larvae, the first weak RFa-lir neurite-like signals of the developing lateral nerve cords are observable (**Figure 3A**– not visible in maximum projection). Originating from the ventral part of the brain ring, they extend along the lateral sides of the larvae. In all parts of the body, but especially concentrated at the anterior pole and around the mouth opening, there are slender elongated RFa-lir neuron-like signals situated between the unstained epidermis cells (**Figure 5D**: *arrowheads* at 7-dpf). Although a connection to the remaining nervous system-like RFa-lir signals is not obvious, their shape and the signal strength comparable to other nervous system-like signals make a function of these cells as receptor cells of a forming peripheral nervous system likely. In the brain ring of 7-dpf larvae, some of the RFa-lir neuron-like signals show neurite-like projections to the epidermal surface (**Supplementary File 5**), further supporting the interpretation of the remaining peripheral signals as receptor cell-like structures.

F-Actin Labeling of Musculature

The first diffuse muscular f-actin signals are detected in larvae of *C. armandi* at 3-dpf (**Figure 4B**: *llm*). They comprise a pair of longitudinally oriented bundles lateral of the midgut. In more advanced stages, these signals become more pronounced and a semi-circular signal behind the posterior rim of the mouth opening is added (**Figure 3B**). By 5-dpf, the lateral f-actin strands have elongated to the anterior and posterior (**Figure 5B**: *llm*). One, later two median dorsal, longitudinal f-actin signals are also visible, extending dorsally from the anterior part of the larva to slightly posterior of the level of the mouth opening (**Figure 5B**: *dlm*). The first f-actin signals of the circular muscles are formed distal of the longitudinal signals, situated in front of and behind the mouth opening (**Figures 3B**, **5B**: *acm* and *pcm*). They seem to be more densely spaced toward the anterior and the posterior end of the larva, respectively (**Figure 5B**). In front of the mouth opening, the circular f-actin signals are completely encircling the larva, whereas the muscular f-actin signals behind the mouth opening are restricted to the dorsal part, extending laterally to the level of the lateral longitudinal muscle strands (**Figure 3B**). In presumably more advanced stages of this age, a pair of diagonally running f-actin signals extends bilaterally from the lateral longitudinal strands anteriorly on each of the dorso-lateral sides of the larva. A second pair of similar, but weaker signals is seen in some specimens more posteriorly (data not shown). These diagonally oriented signals are not addressed as diagonal muscles. Instead, they are seen as forming longitudinal muscles that have not yet assumed their final orientation parallel to the already existing longitudinal strands. The latter assumption is supported by the fact that such diagonal strands are not readily apparent in later stages (see **Figure 5D**).

In *C. mutabilis*, only 5-dpf stages were examined. At this stage, ventro-laterally located, longitudinally oriented strands composed of 2–4 fibers on both sides of the mouth opening are detected (**Figure 5A**: *llm*). A few signals reach from in front of the mouth opening posteriorly, extending along almost the complete length of the larva. Additionally, a median, longitudinal strand, composed of 3–4 paired signals extends along the dorsal side (**Figure 5A**: *dlm*). In this strand, only 1–2 fiber-signals extend the full body length. A group of circular f-actin signals is present in front of the mouth opening (**Figure 5A**: *acm*). The signals are stronger on the dorsal side, diminishing in intensity while extending around the circumference of the larva toward the ventral side. The anterior-most of the signals form complete rings around the larva, whereas the posterior signals form rings that remain open ventrally. A single muscular f-actin signal is observable running alongside the posterior rim of the mouth opening (**Figure 5A**: *bm* and *mo*).

In the oldest observed stages of *C. armandi*, at 7-dpf, the already existing signals have not changed significantly. Only the longitudinal muscle signals on the dorsal side of the larva have slightly increased in intensity and seem to be more evenly spaced. On the ventral side, a buccal muscle becomes apparent behind mouth opening (**Figure 5D**: *bm*). In the posterior half of the body, a set of diagonal signals is seen that encircles the larva in an angle of 30–40° relative to the remaining circular muscles (**Figures 3B**, **5D**: *dm*). It cannot be ruled out that these diagonal signals are derivatives of the circular muscle signals, which they are crossing on the lateral sides of the larva.

Carcinonemertes carcinophila (Monostilifera, Hoplonemertea)

Post-embryonic Development

Although of comparably small size in *C. carcinophila* the opacity of the egg caused by finely dispersed yolk vesicles prevented unambiguous findings by optical examination [transmitted light and confocal laser scanning microscopy (CLSM)] prior to 3 days after egg deposition (*3-dpd*). Since development is somewhat asynchronous even among eggs within the same egg string, some gradual differences in development could be identified when comparing several specimens. Therefore, a superficial overview on early post-embryonic development at 18°C can be given.

In the earliest observable stages at 3-dpd, gastrulation is completed and the blastopore has already closed. The epidermal cells are adorned with multiple cilia showing α-tub-lir. Some invaginations are seen on the apical pole of the developing larva (data not shown). In more advanced stages at 3-dpd, the invagination of the proboscis rudiment and, slightly more ventral, the slender foregut rudiment can be detected as an internal cavity. A connection of the foregut cavity to the midgut cavity could not be clearly seen but its existence cannot be ruled out either. In some specimens, a tuft of elongate cilia emanating from the apical pit is visible (**Figure 6B**: *at* at 4-dpd). At 4-dpd, the larvae have hatched and are pelagic. Apart from the

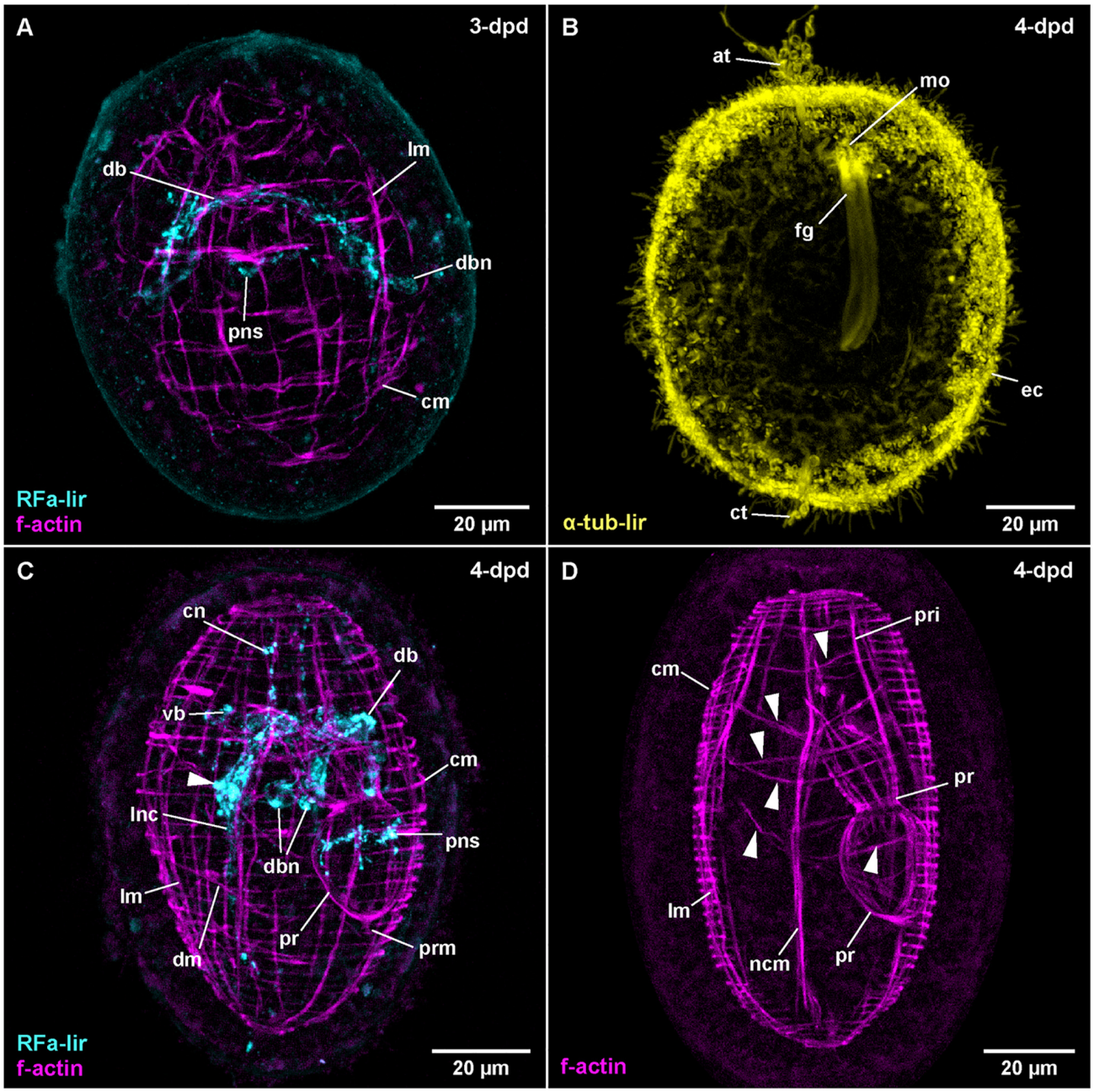

FIGURE 6 | *Carcinonemertes carcinophila* (frontal is up in all images, age of larval stages indicated in top right-hand corner, dpd: days post egg-deposition). **(A)** (RFa-lir: γ = 0.75, f-actin: γ = 0.7); maximum projection of 47 optical sections, dorsal view. **(B)** (γ = 0.6); maximum projection of 26 optical sections, ventro-lateral view. **(C)** (RFa-lir: γ = 0.8, f-actin: γ = 0.7); maximum projection of 45 optical sections, dorso-lateral view. *Arrowhead* indicates neuron-like signal in ventral part of brain ring. **(D)** (γ = 0.75); maximum projection of 21 optical sections, lateral view. *Arrowheads* indicate transversal muscle signals proximal of body wall muscle layers. at: apical tuft, cm: circular muscle, ct: caudal tuft, cn: cephalic neurite-like signal, db: dorsal part of brain ring, dbn: neuron of dorsal part of brain, dm: diagonal muscle, ec: epidermal cilia, fg: foregut, lm: longitudinal muscle, lnc: lateral nerve cord, mo: mouth opening, ncm: nerve cord muscle, pns: proboscis nervous-like signal, pr: proboscis, pri: proboscis insertion muscle, prm: proboscis retractor muscle, vb: ventral part of brain ring.

proboscis invagination and the apical pit, all other epidermal invaginations have disappeared. There is a tuft of elongated cilia emanating from the apical pit (**Figure 6B**: *at*). The foregut is open to the exterior via a mouth opening and there is a caudal tuft at the hind end of the larva visible in some specimens (**Figure 6B**: *fg*, *mo*, and *ct*). At this developmental stage, neither cilia of the midgut epithelium, nor of protonephridia are present. Furthermore, no anal opening or eyes are detected. The larvae

after 4-dpd represent the most advanced developmental stages of *C. carcinophila* studied. Further development of the larva could not be followed due to the lack of older larvae. Moreover, significant metamorphic changes in this ectoparasitic species will supposedly occur after the host, *C. maenas*, has been colonized (*cf.* Stricker and Reed, 1981 for *Carcinonemertes epialti*).

FMRFamide-Like Immunoreactivity

In *C. carcinophila*, the egg-membrane is permeable to antibodies, so that RFa-lir could be detected in developmental stages prior to hatching. In the least developed specimens examined, RFa-lir neurite-like signals can be detected in the future dorsal part of the brain ring (**Figure 6A**: *db*). Along with the neurite-like signals, up to two pairs of dorso-lateral RFa-lir brain neurons are seen (**Figure 6A**: *dbn*). In presumably more advanced stages, the first RFa-lir neurite-like signal in the proboscis rudiment is detectable (**Figure 6A**: *pns*). At this point in time, the lateral nerve cords begin to show short RFa-lir neurite-like signals (**Figure 3C**).

At 4-dpd, the RFa-lir neurite-like signals of the brain ring show it to be completely closed (**Figure 3C**: *vb* and *db*). The number of dorso-lateral neurons posterior of the brain ring has increased to three pairs (**Figure 6C**: *dbn*–only two visible on one body side). Ventral of the brain ring, two pairs of neurons are detected in its vicinity (**Figure 6C**: *arrowhead*) and there is possibly an additional pair anterior of the ventral part of the brain ring present. From the lateral sides of the ventral part of the brain ring, a paired RFa-lir neurite-like signal, presumably the first developing cephalic nerves, extends toward the anterior end of the larva (**Figure 6C**: *cn*). The RFa-lir neurite-like signals of the lateral nerve cords are elongated to the posterior end of the larva, where they connect to each other (**Figure 3C**). In the proboscis, there is a bundle of ring-shaped RFa-lir neurite-like signals in the anterior part of the bulbous region, with associated RFa-lir putative neuron-like signals, one each, ventrally and dorsally (**Figure 6C**: *pns*). In presumably more advanced stages, there seems to be a plexus of weak RFa-lir neurite-like signals underlying the epidermis in the periphery of the larva (data not shown).

F-Actin Labeling of Musculature

The first muscular f-actin signals are detected in 3-dpd stages that are still within the egg membranes. The signals constitute an unordered tangle of obliquely oriented fibers in the vicinity and anterior of the developing lateral nerve cords (as can be shown by double labeling with phalloidin and antibodies against FMRF-amide). The signals are somewhat more densely arranged in the anterior part of the body, as well as on its dorsal side. Judging from their orientation relative to the developing lateral nerve cords, the majority of these signals might be future longitudinal muscle signals, being located distal to the nerve cord signals. Anterior of the developing brain ring, some seemingly transverse signals, arguably future circular muscles are recognized (data not shown). In other still unhatched stages that are assumed to be more advanced, there are more or less evenly spaced longitudinal muscle signals arranged around the circumference of the larva (**Figure 6A**: *lm*). On the dorsal side, the longitudinal signals are more densely set than on the ventral side. Evenly spaced f-actin signals of circular muscles are distributed over the entire length of the larva, although their signals appear slightly weaker on the ventral side (**Figure 6A**: *cm*). In some of these stages the beginning of proboscis muscle development is seen as a bulbous, unordered mass of muscular f-actin signals on the dorsal side but proximal of the longitudinal muscle signals.

In 4-dpd stages, all examined specimens are hatched larvae. The longitudinal body wall muscles comprise evenly spaced signals spanning the complete length of the body that are overlain by the evenly spaced signals of the circular muscles (**Figure 6C**: *lm* and *cm*). The circular signals are also distributed along the complete length of the larva, although they are more densely set than the longitudinal signals (**Figure 6C**: *cm*). In some specimens, a few diagonally oriented f-actin signals located on the ventral side are visible (**Figure 6C**: *dm*), whereas in other, arguably more advanced larvae, the f-actin signals of the diagonal muscles are seen along most of the length of the larva, with most of the signals showing double stranded fiber zones (**Supplementary File 6**). Lateral nerve cord muscles are clearly seen at this stage, extending on the proximal side of the lateral nerve cords, anteriorly passing through the brain ring and ending on both ends of the larva among the body wall muscles (**Figures 6C**, D: *ncm*). The developing proboscis is divided into a posterior, bulbous portion that shows longitudinally oriented muscular f-actin signals only, and an anterior, funnel-shaped portion, that shows both proximal longitudinal and distal circular muscle signals (**Figures 3D**, **6D**: *pr*). Posteriorly, the bulbous portion of the proboscis is connected to the body wall longitudinal muscular signals by the short longitudinal f-actin signal of the proboscis retractor (**Figures 3D**, **6C**: *prm*). Anterior of the funnel-shaped portion, the muscular f-actin signals of the proboscis insertion are represented by a pair of ventro-lateral and a pair of dorso-lateral, longitudinal signals radiating from the anterior rim of the funnel-shaped portion of the developing proboscis the laterally to the body wall muscles (**Figures 3D**, **6D**: *pri*). The ventro-lateral pair runs more or less parallel to the anterior portion of the lateral nerve cord muscle signals. In the same stage, a series of additional transverse muscular f-actin signals are detected proximal of the longitudinal body wall muscles, in the vicinity of the proboscis and foregut (**Figure 6D**: *arrowheads*–not all muscles visible in maximum projection). From anterior to posterior these muscular signals comprise three pairs of dorso-ventral muscles, one strand on each side of the foregut and proboscis rudiment, one u-shaped muscle strand that is dorsally open, a posterior pair of dorso-ventral muscles similar to the anterior three pairs and a posterior u-shaped muscle strand that is open dorsally and forked at its dorsal ends. The function of these muscles can only be speculated about.

Amphiporus sp. (Monostilifera, Hoplonemertea)

Post-embryonic Development

Within one batch of eggs, development was observed to be somewhat asynchronous within a time range of up to 1 day. Therefore, the times of development are approximations for a water temperature of 18°C. After 1-dpd, the majority of

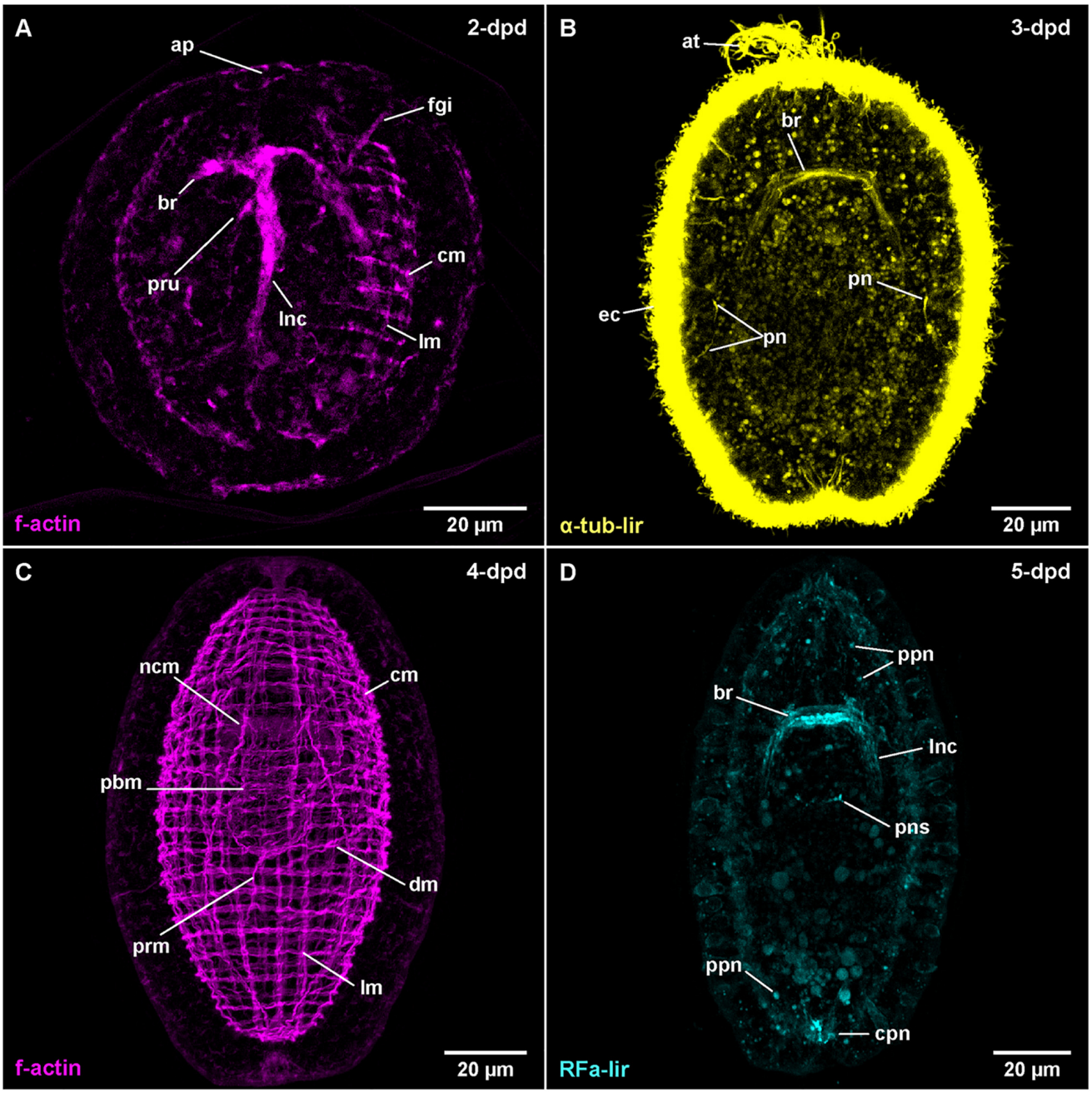

FIGURE 7 | *Amphiporus* sp. (frontal is up in all images, age of larval stages indicated in top right-hand corner, dpd: days post egg-deposition). **(A)** (γ = 1.0); maximum projection of 50 optical sections, ventro-lateral view. **(B)** (γ = 1.1); maximum projection of 15 optical sections, ventral view. **(C)** (γ = 0.7); maximum projection of 46 optical sections, dorsal view. **(D)** (γ = 1.1); maximum projection of 16 optical sections, dorsal view. at: apical tuft, br: brain ring, cm: circular muscle, cpn: caudal peripheral neuron, dm: diagonal muscle, ec: epidermal cilia, fgi: foregut invagination, lm: longitudinal muscle, lnc: lateral nerve cord, ncm: nerve cord muscle, pbm: proboscis muscle, pn: protonephridium, pns: proboscis nervous-like signal, ppn: peripheral plexus neuron, prm: proboscis retractor muscle.

developmental stages have completed gastrulation and the blastopore is closed. At one, presumably the apical pole of the larva, some epidermal invaginations have formed (data not shown). Of these epidermal invaginations, the invagination of the apical pit and, slightly more ventral and deeper, the epidermal in-folding of the developing proboscis remain visible after 2-dpd (**Figure 7A**: *ap* and *pru*). A narrow, elongate inner cavity, located anterior and slightly ventral of the forming proboscis represents the rudiment of the foregut (**Figure 7A**: *fgi*). At 3-dpd, the majority of larvae have hatched and are pelagic, spherical stages completely covered with cilia as shown by α-tub-lir (**Figure 7B** at 3-dpd). They possess a well-developed apical tuft of cilia emanating from the apical pit and a pair of eyes, situated dorso-laterally, slightly posterior of the anterior end of the larva

(data not shown). A pair of simple, unbranched protonephridia is detectable by the cilia of their nephroduct laterally on each side, halfway along the length of the larva (**Figure 7B**: *pn*). After 3-dpd, the anteriorly located, densely ciliated foregut opens to the exterior and a caudal tuft of elongated cilia at the hind-end of the larva begins to form (data not shown). The larvae survived for two additional weeks and became more elongate until they started to degenerate after 18-dpd. At that stage, the mouth opening is still independent of the proboscis pore and a stylet has also not formed yet (data not shown).

FMRFamide-Like Immunoreactivity

Although gastrulation and organogenesis already begin prior to hatching, no immunohistochemical staining could be accomplished owing to the impermeability of the egg-membranes to antibodies. The earliest result of immunohistochemical staining are therefore available for post-hatching stages later than 2-dpd. However, in the subsequent stages, the tissue has a strong autofluorescence that obscures several of the weaker signals in maximum projections of the image series.

The first RFa-lir neurite-like signals that develop are those of the brain ring (**Figure 3C**). It should be noted however, that the signals in the dorsal part of the brain ring are stronger than in the ventral part and the lateral transition from the dorsal to the ventral side of the brain ring showed especially weak signals. Due to strong autofluorescence, RFa-lir neuron-like signals could not be unambiguously identified in the brain ring in early stages. Later, at 4-dpd, a pair of small lateral and 1–3 larger median RFa-lir neuron-like signals are visible anterior of the dorsal part of the brain ring neurite-like signals (**Supplementary File 7**). The lateral nerve cords show RFa-lir neurite-like signals throughout their entire length, as well as, in more advanced stages, a connection in their posterior-most extension (**Figure 3C**). No unambiguously identifiable neuron-like signals along the lateral nerve cord neurite-like signals could be found. Additionally, a semicircular RFa-lir neurite-like signal perpendicular to the longitudinal body axis is detected in the inverted outer epithelium of the developing proboscis. It develops into a ring-shaped, RFa-lir neurite-like signal surrounding the transition zone between the anterior cylindrical and the posterior bulbous part of the developing proboscis by 5-dpd (**Figures 3C**, **7D**: *pns*).

In 5-dpd stage larvae, the overall strength of the brain ring and lateral nerve cord neurite-like signals is slightly increased (**Figure 7D**: *br* and *lnc*). From the brain ring, two pairs of RFa-lir neurite-like signals extend anteriorly, one located ventro-laterally the other dorso-laterally. Several peripheral RFa-lir neuron-like signals are observed at both the anterior, dorsal and the posterior pole of the larva, at the base of the caudal tuft (**Figure 7D**: *cpn*, **Supplementary File 8**). The posterior neuron-like signal aggregation is in close vicinity to the posterior connection of the lateral nerve cords, whereas the anterior neuron-like signal aggregation is in the position where the frontal organ is located in the adult animal. The anterior neuron-like signals are therefore interpreted as the first sensory neurons of the frontal organ. Several peripheral, neuron-like signals are irregularly distributed along the length of the larva (**Figure 7D**: *ppn*). They might represent sensory neurons of a developing peripheral plexus.

After 5-dpd, observation of the nervous system was hampered by difficulties to deliver the antibodies through the body wall musculature to the proximal components of the nervous system without severely compromising the integrity of the larva. Thus, the brain and the lateral nerve cords are comparably weakly stained. In 7-dpd larvae, the epidermis shows a strong fluorescence, so that no internal signals are visible. In the oldest stage (14-dpd), the epidermis shows less intense fluorescence revealing RFa-lir neurite-like signals of the brain ring and the lateral nerve cords (**Figure 8B**: *br* and *lnc*). Anteriorly, the brain and the posterior end of the lateral nerve cords are connected to the anterior and posterior masses of several intensely fluorescent neurite-like and a few neuron-like signals (**Figure 8B**: *fpn* and *cpn*). Both signal aggregations extend from the interior to the surface of the epidermis where they are confluent with the neurite-like signals of a peripheral plexus that extends at the base of numerous, lightly fluorescent epidermal gland cells along the entire body (**Figure 8B**: *pp*). Further development was not observed.

F-Actin Labeling of Musculature and Nervous System

The first f-actin signals labeled with phalloidin are visible in developmental stages at 2-dpd that have not yet hatched from the egg case (**Figure 7A**). The earliest signals detected do not obviously belong to developing muscles but are signals of the developing nervous system, comprising the brain ring and the first rudiments of the lateral nerve cords. In later, but still unhatched stages of this age, fluorescent signals outline a completely developed brain ring that shows stronger signal in its ventral portion and a pair of lateral nerve cords (**Figure 7A**: *br* and *lnc*). The lateral nerve cords, however, do not yet show a posterior connection. Earliest f-actin signals belonging to the body wall muscles are seen as four longitudinally oriented strands, situated in dorso- and ventro-lateral positions, two on each side of the body (data not shown). The signals of the developing longitudinal muscles are weaker in intensity than the signals of the brain and lateral nerve cords. In hatched specimens at 2-dpd, signals of the circular muscles are also detected. They are distributed along the entire length of the larvae and span its circumference on the dorsal and ventral side, thereby showing a gap above the signals of the lateral nerve cords (**Figure 7A**: *cm*, **Supplemetary File 9**). At this stage, the signals of the longitudinal muscles are more numerous but thinner and distributed over the dorsal and ventral sides of the larva (**Figure 7A**: *lm*). However, there are fewer longitudinally extending muscular f-actin signals than there are circular signals.

After 3-dpd, all examined larvae are hatched and both longitudinal and circular muscular f-actin signals are more or less evenly distributed over the larva. The signals of muscular f-actin become more pronounced on the lateral sides of the body and generally stronger than the diffuse f-actin signals of the brain ring and the lateral nerve cords. Both the longitudinal and the lateral signals of the body wall muscles are first arranged in groups of 1–3 (mostly 2) closely set fibers that are evenly spaced from the neighboring groups. The groups of circular signals are more numerous and more densely set than the groups of longitudinal signals. The signals of the longitudinal and circular muscles have significantly increased in intensity in the 4-dpd stages, with the

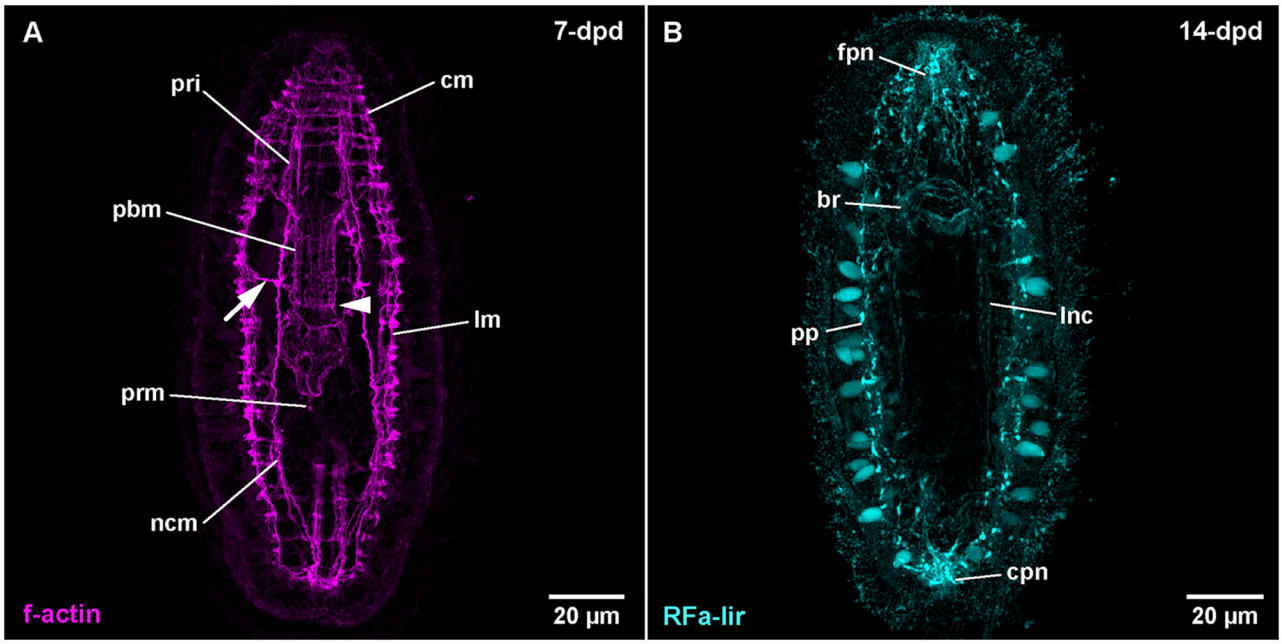

FIGURE 8 | *Amphiporus* sp. (frontal is up in all images, age of larval stages indicated in top right-hand corner, dpd: days post egg-deposition). **(A)** (γ = 0.9); maximum projection of 11 optical sections, ventral view. *Arrowhead* marks sphincter-like f-actin signal in proboscis, *arrow* marks signals extending from nerve cord muscle to body wall muscles. **(B)** (γ = 0.8); maximum projection of 13 optical sections, ventral view. br: brain ring, cm: circular muscle, cpn: caudal peripheral neuron, fpn: frontal peripheral neuron, lm: longitudinal muscle, lnc: lateral nerve cord, ncm: nerve cord muscle, pbm: proboscis muscle, pp: peripheral plexus, pri: proboscis insertion muscle, prm: proboscis retractor muscle.

former also having notably increased in numbers (**Figure 7C**: *lm* and *cm*). The grouped arrangement is still apparent as described before. Adjacent to the diffuse signals of the lateral nerve cords, on their proximal side, there is a single muscular f-actin signal on each side first detected in 3-dpd stages, the signal of the lateral nerve cord muscles, running parallelly to the lateral nerve cords and anteriorly passing through the brain ring (**Figure 7C**: *ncm* at 4-dpd). Anteriorly and posteriorly, the lateral nerve cord muscle signals end at the level of the anterior and posterior end of the body wall muscles, respectively (**Figure 7C**: *ncm*). The lateral nerve cord muscle signals increase in intensity by 4-dpd. In supposedly more advanced stages at 3-dpd and even more obvious at 4-dpd, the first diagonal f-actin signals of the body wall muscles are observed on the ventral and ventro-lateral sides between the circular and the longitudinal signals. The signals run in an angle of 30–45° to the f-actin signals of the circular muscles (**Figure 7C**: *dm*). They comprise few, widely separated fibers along the mid-body region of the larva that cross on the ventral midline in 3-dpd stages and additional weak signals present on the dorsal side of the body on the level of the posterior bulbous part of developing proboscis at 4-dpd. At this stage on the ventral and lateral sides, multiple crisscrossings of diagonal signals are seen **Supplementary File 10**.

The proboscis rudiment shows the first f-actin signals of its muscles as early as 3-dpd. They comprise few weak signals, arranged both longitudinally and circularly around the posterior, bulbous part. They become stronger during subsequent development when distinct longitudinal, some obliquely oriented, and few weak circular muscular f-actin signals around the posterior, bulbous part of the proboscis rudiment form. At the same time, the anteriorly adjacent cylindrical part shows outer circular and inner longitudinal, muscular f-actin signals (**Figures 3D**, **7C**: *pbm* at 4-dpd). One pair of longitudinal muscular f-actin signals extends in the dorsal wall of the anterior, funnel-shaped part of the proboscis, running roughly parallel to the lateral nerve cord muscle signals, which in turn run in the ventral wall of the funnel-shaped part of the developing proboscis apparatus in this body region. The former signals are tentatively addressed as developing proboscis insertion muscles (**Figure 8A**: *pri* at 7-dpd). In addition, at 4-dpf, 1–2 pairs of f-actin signals extend radially from the from the anterior rim of the cylindrical part of the developing proboscis invagination to the body wall muscles (**Supplementary File 10**). A strand of longitudinal muscular f-actin signals belonging to the developing proboscis retractor muscle, extend from the posterior end of the bulbous part of the developing proboscis to the longitudinal body wall muscle signals. It is seen to elongate during further development (**Figure 7C**: *prm*). Other muscular f-actin signals occasionally detected in younger larval stages comprise few transversally and radially oriented thin strands around the proboscis rudiment and the foregut, proximal of the inner longitudinal body wall muscles (not visible in maximum projection). In 4-dpd larvae, a series of muscular f-actin signals around the proboscis apparatus and foregut are detected. They comprise a dorsally open, u-shaped muscle that extends to the dorsal body wall muscles, two pairs of radial signals extending to the lateral body wall muscles, and one pair extending to the anterior body wall muscles. Three pairs of radial muscles are seen running to the dorsal body wall muscles

(not visible in maximum projection, but reminiscent of signals in *C. carcinophila* in **Figure 6D**: *arrowheads*).

The larvae after 4-dpd show a general increase in intensity of the muscular f-actin signals, especially of the body wall muscles. The signals of the diagonal body wall muscles are seen to also cross on the dorsal side at this developmental stage (**Supplementary File 11**). The lateral nerve cord muscle signals are now composed of at least two parallel fibrous signals (**Figure 8A**: *ncm* at 7-dpd). In larval stages at 7-dpd, apart from the muscle signals described for the preceding stages, an additional pair of longitudinal muscular f-actin signals has developed, flanking the foregut on both sided in a proximal position relative to the inner longitudinal body wall muscles (**Supplementary File 12**). In the developing proboscis, a strong ring-shaped muscular f-actin signal is seen that is delimiting the anterior and the posterior half of the middle cylindrical portion of the developing proboscis (**Figure 8A**: *arrowhead*). Occasionally, 1–2 muscular f-actin signals are seen on each side distally extending from the lateral nerve cord muscles to the longitudinal body wall muscle signals in the anterior half of the larva (**Figure 8A**: *arrow*). In successive stages, up to 14-dpd, the existing muscular signals become stronger and especially the cylindrical part of the developing proboscis apparatus becomes more muscular, thus changing its shape to become more or less dumbbell-shaped with its narrowest part being demarcated by the ring-shaped sphincter muscle formed at 7-dpd (data not shown). In the area of the proboscis insertion, additional but weaker longitudinal muscular f-actin signals fan from proximal to distal between the existing stronger longitudinal muscle signals of the proboscis insertion (data not shown). In the most advanced larvae at 18-dpd, before the larvae started to degenerate, no additional muscular systems have formed.

DISCUSSION

Novel Findings on the Development of Body-Wall Muscles and RFa-lir Nervous System

Information on the development of the musculature by means of fluorescent phalloidin labeling and examination with confocal microscopic setups is only available to some detail in the hoplonemertean species *Nemertopsis bivittata*, *Paranemertes peregrina*, and *Pantinonemertes californiensis* (Martindale and Henry, 1995; Maslakova and von Döhren, 2009; Hiebert et al., 2010). In some pilidiophoran species, such as *Maculaura* (as *Micrura*) *alaskensis*, *Lineus ruber*, *Lineus viridis*, and *Micrura wilsoni*, but also the palaeonemertean species *Carinoma tremaphoros*, data on only few stages have been published (Maslakova et al., 2004; Maslakova, 2010b; von Döhren, 2011; Hiebert and Maslakova, 2015b; Martín-Durán et al., 2015). A comparable situation is encountered in the development of the nervous system components with immuno-fluorescent methods, with the serotonin-immunoreactive (*5HT-lir*) component having been subject to more detailed analyses. Data on the development of the 5HT-lir nervous system is available for the pilidiophoran species *M. alaskensis*, *Lineus albocinctus*, as well as an unidentified pilidium-larva of the *gyrans*-type (supposedly *Micrura purpurea*) (Hay-Schmidt, 1990; Maslakova, 2010b; Hindinger et al., 2013); for the hoplonemertean species *Quasitetrastemma stimpsoni* and *P. californiensis* (Chernyshev and Magarlamov, 2010; Hiebert and Maslakova, 2015a); and for the palaeonemertean species *Carinina ochracea* (von Döhren, 2016). Data on the development of the RFa-lir component of the nervous system are scarcer, having only been published for the palaeonemertean species *C. ochracea* and the pilidium larvae of two heteronemertean Pilidiophora, *L. albocinctus* and an unidentified pilidium-larva of the *gyrans*-type, tentatively assigned to *M. purpurea* (Hay-Schmidt, 1990; Hindinger et al., 2013; von Döhren, 2016). To date, no modern investigation has focused on the joint development of body wall musculature and nervous system so that the available data comes from histological examinations only. However, the descriptions are partly contradicting (reviewed in von Döhren, 2015). The present paper reports the first data on the development of the RFa-lir component of the nervous system in two hoplonemertean representatives and significantly expands the knowledge on Palaeonemertea, with data on three additional species.

Development of the RFa-lir Nervous System Is Relatively Uniform in Nemertea but Development of the Body Wall Muscles Differs Significantly

In the examined palaeonemertean species, the first detectable muscular elements are a pair of lateral muscle bundles in the vicinity of the mouth opening in the *C. armandi* and a single short, longitudinal signal dorsally, followed soon after by a pair of lateral bundles in *T. polymorphus*. A similar sequence as in *T. polymorphus* is also suggested for *C. mutabilis*. Furthermore, a muscle ring surrounding the mouth opening becomes apparent in the larva. Subsequently in *T. polymorphus* and *C. armandi*, the muscle strands extend toward anterior and posterior and the lateral bundles seem to distribute dorsally to attain a more or less evenly spaced arrangement of muscle strands along the dorsal and the lateral sides of the body. At the same time the first circular muscle signals appear anterior of the mouth opening on the dorsal side and elongate ventro-laterally. Several additional circular signals appear on the dorsal side anterior and posterior of the first signals. Whereas the circular muscles are added almost up to the anterior tip of the larva, progress of the circular muscles posteriorly stops in front of the mouth opening and an additional region of circular muscle formation appears some distance behind the mouth opening. From here, additional circular muscles are added posteriorly and anteriorly. Data on the development of the body wall musculature in *C. tremaphoros*, although not as detailed, are largely congruent with the herein reported data: longitudinal muscles develop prior to circular muscles in a dorsal to ventral progression and no proboscis muscles are seen to develop in the early larval stage. Circular, but also diagonal muscles have been found in stages as early as 30 h of development (Maslakova et al., 2004). The early formation of the main components of the body wall muscles indicates somewhat faster development in *C. tremaphoros*. Regarding formation of longitudinal body wall muscles with dorsal longitudinal muscles formed prior to

lateral longitudinal muscles, *C. tremaphoros* seems to be more similar to *T. polymorphus* than to *C. armandi*. Outside of Nemertea, this type of body wall muscle formation, especially of the circular component, has never been reported before (*cf.* Wanninger, 2009). In the hoplonemertean species examined, formation of the longitudinal component and shortly afterward the circular component of the body wall muscles seems to be almost synchronous (Maslakova and von Döhren, 2009; Hiebert et al., 2010). In contrast to muscle development in *Amphiporus* sp., *P. peregrina*, and probably also *P. californiensis*, the muscles are not formed in their definite position in *C. carcinophila* but seem to become evenly distributed later during the course of development to constitute the definite orthogonal arrangement of circular and longitudinal muscle strands. Both the longitudinal and circular muscles are fully formed at the time of hatching. The diagonal muscles in the hoplonemertean species examined develop after hatching *in situ*; in *C. carcinophila* and *Amphiporus* sp. most likely, if not as independent entities, as derivatives of the longitudinal musculature. While the muscles of the proboscis apparatus and the lateral nerve cord muscles develop shortly after the larva has hatched in the hoplonemertean species, there is no sign of proboscis muscle development in any of the examined palaeonemertean species during the observed development.

No signs of differentiated nervous systems could be detected by immunolabelling with antibodies against FMRFamide in the newly hatched larvae of the examined palaeonemertean species. It is only later in the elongating larvae that the brain ring, the neurite bundles around the mouth opening and subsequently, the lateral nerve cords and a peripheral plexus develop. Even in the most advanced stages investigated, no trace of neuronal elements of the future proboscis apparatus was seen. In *C. ochracea*, the only other palaeonemertean species investigated for the development of the RFa-lir nervous system the sequence of formation is nearly identical. Development of the RFa-lir nervous system component is first seen in the dorsal portion of the brain ring and progresses from there to the ventral side of the larva, where the ventral portion of the brain ring forms and the lateral nerve cords develop. Also, the distribution of neuronal perikarya is essentially the same (von Döhren, 2016). The early appearance of a longitudinal RFa-lir dorsal nerve is a character *C. ochracea* shares with *T. polymorphus*, it is not seen to form in the examined *Carinoma* species, although they possess dorsal nerves as adults (Beckers et al., 2013). In both *C. carcinophila* and *Amphiporus* sp., the brain ring begins to form before hatching, although in *C. carcinophila*, like in the palaeonemertean species studied, formation of the dorsal part precedes that of the ventral part (this study and von Döhren, 2016). The lateral nerve cords are fully developed at the time of hatching in *Amphiporus* sp. and shortly after in *C. carcinophila*. Development of the proboscis nervous system, on the other hand, seems to begin earlier in *C. carcinophila*. Only the peripheral nerve plexus begins to develop after the larva has hatched in both species.

In Pilidiophora, the nervous system is described to develop with the brain ring forming prior to the development of the lateral nerve cords, and thus in a similar way as described for palaeonemertean and hoplonemertean species (reviewed in von Döhren, 2015). Development of the RFa-lir component of the peptidergic nervous system is unfortunately not detailed enough to allow for comparison of the developmental sequence (Hindinger et al., 2013). With the exception of *L. ruber* that has a derived intracapsular larval type, the development of the body wall muscles in Pilidiophora, has not been subject to detailed, comparative investigations using fluorescent staining and confocal microscopy observations (Martín-Durán et al., 2015). In *L. ruber* and *L. viridis*, the larval tissues are devoid of musculature and juvenile muscles begin to develop late, shortly before the larval envelope is shed (von Döhren, 2011; Martín-Durán et al., 2015). In the former species the first differentiated muscles are detected around the mouth opening and in the cephalic lobe, followed later by the body wall muscles and the musculature of the pharynx (Martín-Durán et al., 2015). In the various histological investigations, there seems to be some discord as to whether the longitudinal or the circular component of the body wall muscles develops first, but all studies agree in that the body wall muscles of the juvenile are formed independently of the larval musculature of the pilidium (reviewed in von Döhren, 2015). Clearly, a closer look at the development of the musculature of pilidiophoran species with immunofluorescent staining and CLSM would refine the picture and help resolve the prevailing contradiction in the descriptions.

Heterochronic Effects in Neuromuscular System-Development Might Be Correlated With Morphological Diversity in the Adults

The diversity in the development of muscles and nervous system in the investigated nemertean species differs most strikingly in the degree of differentiation of the respective organ systems at the time of hatching. In palaeonemertean larvae, the first muscular and RFa-lir nervous elements are formed in the larva after hatching. The main difference between the two palaeonemertean species examined lies in the timing of development of the body wall musculature. Relative to the developing RFa-lir nervous system, development of the body wall muscles starts considerably later in *T. polymorphus* than in *Carinoma* species (this study and Maslakova et al., 2004). Presently, it remains unclear whether this difference represents an acceleration in *C. armandi* or a deceleration in *T. polymorphus*. In hoplonemertean larvae, the timing of development of the respective organ systems is rather different. According to published results on *P. peregrina* and *P. californiensis*, the main components of the body wall muscles develop in the early pelagic larval stage after hatching (Maslakova and von Döhren, 2009; Hiebert et al., 2010), whereas in *C. carcinophila* and *Amphiporus* sp., most of the body wall musculature have already formed before the larva hatches. With the nearly synchronous mode of muscle formation, the only true difference between the herein described species on the one hand and *P. peregrina* and *P. californiensis* on the other hand, seems to be the time of hatching, that is delayed in *Amphiporus* sp. and *C. carcinophila*. For the development of the RFa-lir component of the peptidergic nervous system in Hoplonemertea, there was no detailed-enough comparative data available prior to this investigation. In the palaeonemertean species *C. ochracea*, *T. polymorphus* and the *Carinoma* species, the RFa-lir component

of the brain ring and the lateral longitudinal nerve cords develop after the larvae have hatched (this stuy and von Döhren, 2016). In *C. carcinophila* and *Amphiporus* sp. on the other hand, the RFa-lir component is already beginning to differentiate before hatching. Further investigations in other hoplonemertean species will have to show whether the onset of the formation of the RFA-lir component of the nervous system similarly coincides with onset of muscle formation or starts earlier, as seen in *T. polymorphus*.

Irrespective of the developmental progress at hatching, development of the neuromuscular system in Hoplonemertea shows a heterochronic shift compared to Palaeonemertea and Pilidiophora. The components of the proboscis muscles and nervous system, which are clearly adult structures, form before or soon after hatching in Hoplonemertea (this study and Maslakova and von Döhren, 2009; Chernyshev and Magarlamov, 2010; Hiebert et al., 2010; Hiebert and Maslakova, 2015a). A general acceleration of development in Hoplonemertea compared to Palaeonemertea and Pilidiophora and thus considerably shorter time needed for metamorphosis in hoplonemertean species, has long been known for Nemertea, (Iwata, 1960). Interestingly, morphological diversity with respect to the nervous system and musculature seems to be negatively correlated with the duration of post-embryonic development. Hoplonemertean larvae, in which development is accelerated, show comparably uniform adult neuromuscular morphologies. In palaeonemertean and pilidiophoran species, formation of juvenile structures takes much longer (Iwata, 1960; Maslakova, 2010b; Beckers et al., 2015). On the other hand, morphological diversity of musculature and nervous system, e.g., proboscis musculature and brain anatomy, is much higher in these lineages (Chernyshev, 2010, 2015; Beckers et al., 2013, 2018; Beckers, 2015). It remains to be shown if this different diversity observed is due to developmental timing or if acceleration of the formation of prospective adult structures in Hoplonemertea was only made possible because of relatively uniform morphology in the first place.

No Transitory Muscle or RFa-lir Nervous System Elements Are Detected in Palaeo- or Hoplonemertean Larvae

In recent years, employing fluorescent and immunofluorescent methods to follow the development of spiralian larvae has led to an enormous increase of comparative data in a number of clades, foremost in Annelida and Mollusca, but also in Lophophorata, Entoprocta, and Platyhelminthes (Temereva, 2012; Temereva and Wanninger, 2012; Temereva and Tsitrin, 2013, 2014; Sonnleitner et al., 2014; Audino et al., 2015; Bleidorn et al., 2015; Scherholz et al., 2015; Wanninger, 2015; Wanninger and Wollesen, 2015; Kristof et al., 2016; Sun et al., 2019). However, whereas patterns are emerging in the more well-studied clades, others, such as Nemertea, remained largely unknown from a comparative perspective.

Among Lophotrochozoa (*s. str.*), the most prevalent type of larva is the trochophore-type larva that has therefore been suggested to represent the ancestral lophotrochozoan larval form (Marlow et al., 2014; Nielsen, 2018; Malakhov et al., 2019; Wang et al., 2020). With comparably few, arguably derived exceptions, the trochophore-type larva and its presumably related forms, such as the actinotrocha-larva of Phoronida, and the different larval-types of Brachiopoda, Ectoprocta, and Entoprocta, show certain comparable, and hence assumingly homologous, muscular and neural structures (Wanninger, 2008, 2009; Nielsen, 2012, 2013, 2015). They comprise: (1) the prototroch muscle ring, a ring muscle underlying the prototroch (an equatorial band of cells adorned with differentially elongated, compound cilia); (2) the trochal neurite (bundle), a neurite or neurite-bundle that runs alongside the prototroch ring muscle; and (3) the apical organ comprising a group of cells, some with apical extensions that project into the apical pit or in its vicinity. The apical organ is minimally composed of a small to moderate number of flask-shaped 5HT-lir and a small number of RFa-lir cells (Wanninger, 2008). All of these structures are considered larval, since they commonly develop early in development and disappear later, during metamorphosis. In Nemertea, the pilidium has been, until more recently, assumed to represent the larval type that is homologous to the trochophore-type larva. Therefore, the nervous and muscular elements of the apical pit and the marginal band in the pilidium and the trochophore-type larva were interpreted as homologous (Nielsen, 2005, 2012). However, molecular phylogenetic analyses have clearly shown that the pilidium is restricted to the taxon Pilidiophora, which in turn represents a derived clade within Nemertea (Thollesson and Norenburg, 2003; Andrade et al., 2014). Therefore, it is more parsimonious that the pilidium larva is not the ancestral larval form of Nemertea. As a consequence, musculature and nervous system of the pilidium are most likely not homologous to respective structures in the trochophore-like larval type (Maslakova and Hiebert, 2014).

The absence of elaborated larval structures, such as the prototroch in larvae of Palaeonemertea and Hoplonemertea is reflected by the development of the nervous system and body-wall muscles. Whereas the first muscular element to develop in most lophotrochozoan larvae is the larval prototroch muscle ring (Wanninger, 2009; Bleidorn et al., 2015), the first muscles to develop in nemertean larvae are the longitudinal muscles of the body wall (this study and Maslakova et al., 2004; Maslakova and von Döhren, 2009; Hiebert et al., 2010; von Döhren, 2015). The circular muscles anterior of the mouth opening that develop subsequently in palaeonemertean species are different from the prototroch muscle ring of trochophore-type larvae in that they are located a noticeable distance away from the mouth opening instead of adjacent to the mouth opening as in most feeding trochophore-type larvae. Additionally, they are, unlike the prototroch muscle ring, obviously not transitory muscles (this study). Neither in hoplonemertean nor in palaeonemertean larvae, RFa-lir trochal neurites have been observed (this study and von Döhren, 2016). The brain ring in Palaeonemertea is seen to form from putative neuroblasts presumably originating from the apical pit and later the paired lateral nerve cords develop from its ventral portion. A similar sequence of development is described for the 5HT-lir component of the nervous system, although development starts in the ventral portion of the brain ring (von Döhren, 2016). The identity of the brain ring as a

non-larval structure becomes evident from its position in the hoplonemertean larvae, in which it surrounds the developing proboscis and, at the same time, is located posterior to the mouth opening; an arrangement that is identically found in adults of Hoplonemertea (Maslakova and von Döhren, 2009; Beckers et al., 2018). The early developing ring-shaped brain is thus clearly different and not comparable with the trochal neurites or neurite bundles of trochophore-type larvae.

Although an apical pit with an apical tuft of cilia is present in the trochophore-type larva as well as in all planktonic larval types of nemerteans, the respective expressions of RFa-lir neurons are clearly different. In many trochophore-type larvae, the apical organ neurons show RFa-lir early in development and the RFa-lir component of the brain develops later in close vicinity to the apical neurons (Wanninger, 2009). In nemertean larvae, no comparably clear signal of RFa-lir expressing apical neurons is detectable. In larvae of the examined palaeonemertean species, faint signals are seen instead, that have disappeared when the first clear signals of the future dorsal part of the RFa-lir component of the brain ring are visible (this study). Due to their faint and very short expression, these signals are interpreted as yet undifferentiated RFa-lir brain neurons that invade the larva from the apical pit and its vicinity. They are thus most likely identical to the first clearly visible RFa-lir neuron-like signals of the dorsal brain ring. Although this does not preclude the RFa-lir apical neurons of the trochophore-type larva from being homologous to the faint early RFa-lir signals in palaeonemertean larvae as neuroblasts, their respective developmental fate cannot be considered truly homologous. Later developing peripheral RFa-lir neurons with presumably sensory function in both palaeonemertean and hoplonemertean larvae should be interpreted as components of the developing peripheral plexus, that is also present in the adults and therefore not a transitory larval trait homologous to the early apical neurons of lophotrochozoan larvae.

CONCLUSION

Details on the developmental diversity in Nemertea are only starting to become known. However, some interesting aspects are emerging that deserve to be pursued in the future–in Nemertea but also beyond:

(1) Most of within clade morphological diversity in Nemertea seems to result from post-embryonic development. Future research needs to concentrate on the mechanisms that generate the morphological diversity.
(2) Acceleration of development seems to be correlated with decreasing morphological diversity in Hoplonemertea. It remains to be investigated, which is the cause and which is the result and whether this correlation also holds true on a larger scale.
(3) The hypothetical, ancestral nemertean larva seems to lack strictly larval structures in the investigated neuromuscular system components. Whether this lack is ancestral or derived with respect to the assumingly ancestral trochophore-type larva of Lophotrochozoa can only be answered when a robust placement of Nemertea within the phylogeny of Spiralia is available.

DATA AVAILABILITY STATEMENT

The original contributions presented in the study are included in the article/**Supplementary Material**, further inquiries can be directed to the corresponding author.

AUTHOR CONTRIBUTIONS

The author confirms being the sole contributor of this work and has approved it for publication.

FUNDING

The work at Friday Harbor Laboratories was financially supported by a German Research Council-grant (DFG: Ba 2015/11-1) and the work at the Station Biologique de Roscoff was made possible with financial support by the ASSEMBLE Marine program of the EU ("Comparative development in Nemerteans").

ACKNOWLEDGMENTS

I would like to gratefully acknowledge the staff of the Friday Harbor Laboratories, and especially S. A. Maslakova for assistance with collecting and fertilizing of *Carinoma mutabilis* and rearing, staining and imaging of the larvae of this species. I would also like to express my gratitude to the staff of the Station de Biologie Marine de Concarneau, for offering hospitality during the collecting trips for *Carinoma armandi*, the staff of the Wattenmeerstation of the AWI Bremerhaven in List auf Sylt, including the crew of the research vessel "Mya" for providing laboratory facilities and conducting collecting cruises for *Carcinonemertes carcinophila*, and the staff of the Station Biologique de Roscoff for providing equipment and laboratory facilities for collecting and fertilizing *Tubulanus polymorphus* and rearing the larvae of this species. I would also like to thank T. Bartolomaeus for helping to collect several of the included species and C. Müller from the Institute of Evolutionary Biology and Ecology of the University of Bonn for staining and imaging of larvae of *Amphiporus* sp., *C. armandi*, *C. carcinophila*, and *T. polymorphus*. The editor and the reviewers are gratefully acknowledged for helpful comments.

SUPPLEMENTARY MATERIAL

The Supplementary Material for this article can be found online at: https://www.frontiersin.org/articles/10.3389/fevo.2021.654846/full#supplementary-material

Supplementary Table 1 | Adjustments of CLSM-stacks made with Fiji (ImageJ version 1.53c).

Supplementary File 1 | fly-through video of image stack of *Tubulanus polymorphus* 4-dpf, same as in **Figure 1C**.

Supplementary File 2 | fly-through video of image stack of *Tubulanus polymorphus* 6-dpf, same as in **Figure 2A**.

Supplementary File 3 | fly-through video of image stack of *Carinoma armandi* 2-dpf, RFa-lir, frontal is up.

Supplementary File 4 | fly-through video of image stack of *Carinoma armandi* 5-dpf, RFa-lir of specimen in **Figure 5B**.

Supplementary File 5 | fly-through video of image stack of *Carinoma armandi* 7-dpf, RFa-lir of specimen in **Figure 5D**.

Supplementary File 6 | fly-through video of image stack of *Carcinonemertes carcinophila* 4-dpd, f-actin stain of specimen in **Figure 6C**.

Supplementary File 7 | fly-through video of image stack of *Amphiporus* sp. 4-dpd, RFa-lir of specimen in **Figure 7C**.

Supplementary File 8 | fly-through video of image stack of *Amphiporus* sp. 5-dpd, same as **Figure 7D**.

Supplementary File 9 | fly-through video of image stack of *Amphiporus* sp. 2-dpd, same as **Figure 7A**.

Supplementary File 10 | fly-through video of image stack of *Amphiporus* sp. 4-dpd, same as **Figure 7C**.

Supplementary File 11 | fly-through video of image stack of *Amphiporus* sp. 5-dpd, f-actin stain of specimen in **Figure 7D**.

Supplementary File 12 | fly-through video of image stack of *Amphiporus* sp. 7-dpd, same as **Figure 8A**.

REFERENCES

Aguinaldo, A. M. A., Turbeville, J. M., Linford, L. S., Rivera, M. C., Garey, J. R., Raff, R. A., et al. (1997). Evidence for a clade of nematodes, arthropods and other moulting animals. *Nature* 387, 489–493. doi: 10.1038/387489a0

Altenburger, A., and Wanninger, A. (2009). Comparative larval myogenesis and adult myoanatomy of the rhynchonelliform (articulate) brachiopods *Argyrotheca cordata, A. cistellula*, and *Terebratalia transversa*. *Front. Zool.* 6:3. doi: 10.1186/1742-9994-6-3

Altenburger, A., and Wanninger, A. (2010). Neuromuscular development in *Novocrania anomala*: evidence for the presence of serotonin and a spiralian-like apical organ in lecithotrophic brachiopod larvae. *Evol. Dev.* 12, 16–24. doi: 10.1111/j.1525-142X.2009.00387.x

Andrade, S. C. S., Montenegro, H., Strand, M., Schwartz, M. L., Kajihara, H., Norenburg, J. L., et al. (2014). A transcriptomic approach to ribbon worm systematics (Nemertea): resolving the pilidiophora problem. *Mol. Biol. Evol.* 31, 3206–3215. doi: 10.1093/molbev/msu253

Andrade, S. C. S., Strand, M., Schwartz, M., Chen, H., Kajihara, H., von Döhren, J., et al. (2012). Disentangling ribbon worm relationships: multi-locus analysis supports traditional classification of the phylum Nemertea. *Cladistics* 28, 141–159. doi: 10.1111/j.1096-0031.2011.00376.x

Audino, J. A., Marian, J. E. A. R., Kristof, A., and Wanninger, A. (2015). Inferring muscular ground patterns in Bivalvia: myogenesis in the scallop *Nodipecten nodosus*. *Front. Zool.* 12:34. doi: 10.1186/s12983-015-0125-x

Beckers, P. (2015). The nervous systems of Pilidiophora (Nemertea). *Zoomorphology* 134, 1–24. doi: 10.1007/s00435-014-0246-3

Beckers, P., and von Döhren, J. (2015). "Nemertea (Nemertini)," in *Structure and Evolution of Invertebrate Nervous Systems*, eds A. Schmidt-Rhaesa, S. Harzsch, and G. Purschke (Oxford: Oxford University Press), 148–165.

Beckers, P., Loesel, R., and Bartolomaeus, T. (2013). The nervous systems of basally branching Nemertea (Palaeonemertea). *PLoS One* 8:e66137. doi: 10.1371/journal.pone.0066137

Beckers, P., Bartolomaeus, T., and von Döhren, J. (2015). Observations and experiments on the biology and life history of *Riseriellus occultus* (Heteronemertea: Lineidae). *Zoolog. Sci.* 32, 531–546. doi: 10.2108/zs140270

Beckers, P., Krämer, D., and Bartolomaeus, T. (2018). The nervous systems of Hoplonemertea (Nemertea). *Zoomorphology* 137, 473–500. doi: 10.1007/s00435-018-0414-y

Bleidorn, C., Helm, C., Weigert, A., and Aguado, M. T. (2015). "Annelida," in *Evolutionary Developmental Biology of Invertebrates Vol. 2: Lophotrochozoa (Spiralia)*, ed. A. Wanninger (Wien: Springer), 193–230.

Boyer, B. C., and Henry, J. Q. (1998). Evolutionary modifications of the spiralian developmental program. *Integr. Comp. Biol.* 38, 621–633. doi: 10.1093/icb/38.4.621

Chernyshev, A. V. (2000). Food and feeding behavior of the nemertean *Tortus tokmakovae*. *Russ. J. Mar. Biol.* 26, 120–123. doi: 10.1007/BF02759525

Chernyshev, A. V. (2010). Confocal laser scanning microscopy analysis of the phalloidin-labelled musculature in nemerteans. *J. Nat. Hist.* 44, 2287–2302. doi: 10.1080/00222933.2010.504890

Chernyshev, A. V. (2015). CLSM analysis of the phalloidin-stained muscle system of the nemertean proboscis and rhynchocoel. *Zoolog. Sci.* 32, 547–560. doi: 10.2108/zs140267

Chernyshev, A. V., Astakhova, A. A., Dautov, S. S., and Yushin, V. V. (2013). The morphology of the apical organ and adjacent epithelium of *pilidium prorecurvatum*, a pelagic larva of an unknown heteronemertean (Nemertea). *Russ. J. Mar. Biol.* 39, 116–124. doi: 10.1134/S106307401302003x

Chernyshev, A. V., and Magarlamov, T. Y. (2010). The first data on the nervous system of hoplonemertean larvae (Nemertea, Hoplonemertea). *Dokl. Biol. Sci.* 430, 48–50. doi: 10.1134/S001249661001

Dunn, C. W., Giribet, G., Edgecombe, G. D., and Hejnol, A. (2014). Animal phylogeny and its evolutionary implications. *Annu. Rev. Ecol. Evol. Syst.* 45, 371–395. doi: 10.1146/annurev-ecolsys-120213-091627

Dunn, C. W., Hejnol, A., Matus, D. Q., Pang, K., Browne, W. E., Smith, S. A., et al. (2008). Broad phylogenomic sampling improves resolution of the animal tree of life. *Nature* 452, 745–749. doi: 10.1038/nature06614

Edgecombe, G. D., Giribet, G., Dunn, C. W., Hejnol, A., Kristensen, R. M., Neves, R. C., et al. (2011). Higher-level metazoan relationships: recent progress and remaining questions. *Org. Divers. Evol.* 11, 151–172. doi: 10.1007/s13127-011-0044-4

Giribet, G. (2002). Current advances in the phylogenetic reconstruction of metazoan evolution. A new paradigm for the cambrian explosion? *Mol. Phylogenet. Evol.* 24, 345–357. doi: 10.1016/S1055-7903(02)00206-3

Giribet, G. (2016). New animal phylogeny: future challenges for animal phylogeny in the age of phylogenomics. *Org. Divers. Evol.* 16, 419–426. doi: 10.1007/s13127-015-0236-4

Gruhl, A. (2008). Muscular systems in gymnolaemate bryozoan larvae (Bryozoa: Gymnolaemata). *Zoomorphology* 127, 143–159. doi: 10.1007/s00435-008-0059-3

Gruhl, A. (2009). Serotonergic and FMRFamidergic nervous systems in gymnolaemate bryozoan larvae. *Zoomorphology* 128, 135–156. doi: 10.1007/s00435-009-0084-x

Halanych, K. M., Bacheller, J. D., Aguinaldo, A. M., Liva, S. M., Hillis, D. M., and Lake, J. A. (1995). Evidence from 18S ribosomal DNA that the lophophorates are protostome animals. *Science* 267, 1641–1643. doi: 10.1126/science.7886451

Hay-Schmidt, A. (1990). Catecholamine-containing, serotonin-like and neuropeptide FMRFamide-like immunoreactive cells and processes in the nervous system of the pilidium larva (Nemertini). *Zoomorphology* 109, 231–244. doi: 10.1007/BF00312190

Hejnol, A., Obst, M., Stamatakis, A., Ott, M., Rouse, G. W., Edgecombe, G. D., et al. (2009). Assessing the root of bilaterian animals with scalable phylogenomic methods. *Proc. R. Soc. B Biol. Sci.* 276, 4261–4270. doi: 10.1098/rspb.2009.0896

Hiebert, L. S., and Maslakova, S. A. (2015a). Expression of *Hox, Cdx*, and *Six3/6* genes in the hoplonemertean *Pantinonemertes californiensis* offers insight into the evolution of maximally indirect development in the phylum Nemertea. *Evodevo* 6:26. doi: 10.1186/s13227-015-0021-7

Hiebert, T. C., and Maslakova, S. A. (2015b). Larval development of two NE Pacific pilidiophoran nemerteans (Heteronemertea; Lineidae). *Biol. Bull.* 229, 265–275.

Hiebert, L. S., Gavelis, G., von Dassow, G., and Maslakova, S. A. (2010). Five invaginations and shedding of the larval epidermis during development of the hoplonemertean *Pantinonemertes californiensis* (Nemertea: Hoplonemertea). *J. Nat. Hist.* 44, 2331–2347. doi: 10.1080/00222933.2010.504893

Hindinger, S., Schwaha, T., and Wanninger, A. (2013). Immunocytochemical studies reveal novel neural structures in nemertean pilidium larvae and provide

evidence for incorporation of larval components into the juvenile nervous system. *Front. Zool.* 10:31. doi: 10.1186/1742-9994-10-31

Iwata, F. (1960). Studies on the comparative embryology of nemerteans with special reference to their interrelationships. *Publ. Akkeshi Mar. Biol. Stn.* 10, 1–55.

Kajihara, H., Chernyshev, A. V., Sun, S.-C., Sundberg, P., and Crandall, F. B. (2008). Checklist of nemertean genera and species published between 1995 and 2007. *Species Divers.* 13, 245–274. doi: 10.12782/specdiv.13.245

Kocot, K. M. (2016). On 20 years of Lophotrochozoa. *Org. Divers. Evol.* 16, 329–343. doi: 10.1007/s13127-015-0261-3

Kocot, K. M., Struck, T. H., Merkel, J., Waits, D. S., Todt, C., Brannock, P. M., et al. (2017). Phylogenomics of lophotrochozoa with consideration of systematic error. *Syst. Biol.* 66, 256–282. doi: 10.1093/sysbio/syw079

Kristof, A., de Oliveira, A. L., Kolbin, K. G., and Wanninger, A. (2016). Neuromuscular development in Patellogastropoda (Mollusca: Gastropoda) and its importance for reconstructing ancestral gastropod bodyplan features. *J. Zool. Syst. Evol. Res.* 54, 22–39. doi: 10.1111/jzs.12112

Kvist, S., Laumer, C. E., Junoy, J., and Giribet, G. (2014). New insights into the phylogeny, systematics and DNA barcoding of Nemertea. *Invertebr. Syst.* 28, 287–308. doi: 10.1071/IS13061

Lambert, J. D. (2010). Developmental patterns in spiralian embryos. *Curr. Biol.* 20, R72–R77. doi: 10.1016/j.cub.2009.11.041

Laumer, C. E., Bekkouche, N., Kerbl, A., Goetz, F., Neves, R. C., Sørensen, M. V., et al. (2015). Spiralian phylogeny informs the evolution of microscopic lineages. *Curr. Biol.* 25, 2000–2006. doi: 10.1016/j.cub.2015.06.068

Laumer, C. E., Fernández, R., Lemer, S., Combosch, D., Kocot, K. M., Riesgo, A., et al. (2019). Revisiting metazoan phylogeny with genomic sampling of all phyla. *Proc. R. Soc. B Biol. Sci.* 286:20190831. doi: 10.1098/rspb.2019.0831

Malakhov, V. V., Bogomolova, E. V., Kuzmina, T. V., and Temereva, E. N. (2019). Evolution of metazoan life cycles and the origin of pelagic larvae. *Russ. J. Dev. Biol.* 50, 303–316. doi: 10.1134/S1062360419060043

Marlétaz, F., Peijnenburg, K. T. C. A., Goto, T., Satoh, N., and Rokhsar, D. S. (2019). A new spiralian phylogeny places the enigmatic arrow worms among gnathiferans. *Curr. Biol.* 29, 312–318.e3. doi: 10.1016/j.cub.2018.11.042

Marlow, H., Tosches, M. A., Tomer, R., Steinmetz, P. R., Lauri, A., Larsson, T., et al. (2014). Larval body patterning and apical organs are conserved in animal evolution. *BMC Biol.* 12:7. doi: 10.1186/1741-7007-12-7

Martín-Durán, J. M., and Marlétaz, F. (2020). Unravelling spiral cleavage. *Development* 147:dev181081. doi: 10.1242/dev.181081

Martín-Durán, J. M., Vellutini, B. C., and Hejnol, A. (2015). Evolution and development of the adelphophagic, intracapsular Schmidt's larva of the nemertean *Lineus ruber*. *Evodevo* 6:28. doi: 10.1186/s13227-015-0023-5

Martindale, M. Q., and Henry, J. Q. (1995). Modifications of cell fate specification in equal-cleaving nemertean embryos - alternate patterns of spiralian development. *Development* 121, 3175–3185.

Maslakova, S. A. (2010a). The invention of the pilidium larva in an otherwise perfectly good spiralian phylum Nemertea. *Integr. Comp. Biol.* 50, 734–743. doi: 10.1093/icb/icq096

Maslakova, S. A. (2010b). Development to metamorphosis of the nemertean pilidium larva. *Front. Zool.* 7:30. doi: 10.1186/1742-9994-7-30

Maslakova, S. A., and Hiebert, T. C. (2014). From trochophore to pilidium and back again- a larva's journey. *Int. J. Dev. Biol.* 58, 585–591. doi: 10.1387/ijdb.140090sm

Maslakova, S. A., and von Döhren, J. (2009). Larval development with transitory epidermis in *Paranemertes peregrina* and other hoplonemerteans. *Biol. Bull.* 216, 273–292. doi: 10.2307/25548160

Maslakova, S. A., Martindale, M. Q., and Norenburg, J. L. (2004). Vestigial prototroch in a basal nemertean, *Carinoma tremaphoros* (Nemertea; Palaeonemertea). *Evol. Dev.* 6, 219–226. doi: 10.1111/j.1525-142X.2004.04027.x

McDermott, J. J., and Roe, P. (1985). Food, feeding behavior and feeding ecology of nemerteans. *Am. Zool.* 25, 113–125. doi: 10.1093/icb/25.1.113

Nezlin, L. (2010). The golden age of comparative morphology: laser scanning microscopy and neurogenesis in trochophore animals. *Russ. J. Dev. Biol.* 41, 381–390. doi: 10.1134/S1062360410060056

Nielsen, C. (2004). Trochophora Larvae: cell-Lineages, ciliary bands, and body regions. 1. Annelida and Mollusca. *J. Exp. Zool. Part B Mol. Dev. Evol.* 302, 35–68. doi: 10.1002/jez.b.20001

Nielsen, C. (2005). Trochophora larvae: cell-lineages, ciliary bands and body regions. 2. Other groups and general discussion. *J. Exp. Zool. Part B Mol. Dev. Evol.* 304, 401–447. doi: 10.1002/jez.b.21050

Nielsen, C. (2010). Some aspects of spiralian development. *Acta Zool.* 91, 20–28. doi: 10.1111/j.1463-6395.2009.00421.x

Nielsen, C. (2012). How to make a protostome. *Invertebr. Syst.* 26, 25–40. doi: 10.1071/IS11041

Nielsen, C. (2013). Life cycle evolution: was the eumetazoan ancestor a holopelagic, planktotrophic gastraea? *BMC Evol. Biol.* 13:171. doi: 10.1186/1471-2148-13-171

Nielsen, C. (2015). Larval nervous systems: true larval and precocious adult. *J. Exp. Biol.* 218, 629–636. doi: 10.1242/jeb.109603

Nielsen, C. (2018). Origin of the trochophora larva. *R. Soc. Open Sci.* 5:180042. doi: 10.1098/rsos.180042

Nielsen, C., and Worsaae, K. (2010). Structure and occurrence of cyphonautes larvae (Bryozoa, Ectoprocta). *J. Morphol.* 271, 1094–1109. doi: 10.1002/jmor.10856

Richter, S., Stach, T., and Wanninger, A. (2015). "Perspective — nervous system development in bilaterian larvae: testing the concept of 'primary larvae," in *Structure and Evolution of Invertebrate Nervous Systems*, eds A. Schmidt-Rhaesa, S. Harzsch, and G. Purschke (Oxford: Oxford University Press), 313–324.

Santagata, S. (2004). Larval development of *Phoronis pallida* (Phoronida): implications for morphological convergence and divergence among larval body plans. *J. Morphol.* 259, 347–358. doi: 10.1002/jmor.10205

Santagata, S. (2008a). Evolutionary and structural diversification of the larval nervous system among marine bryozoans. *Biol. Bull.* 215, 3–23. doi: 10.2307/25470679

Santagata, S. (2008b). The morphology and evolutionary significance of the ciliary fields and musculature among marine bryozoan larvae. *J. Morphol.* 269, 349–364. doi: 10.1002/jmor.10592

Santagata, S. (2011). Evaluating neurophylogenetic patterns in the larval nervous systems of brachiopods and their evolutionary significance to other bilaterian phyla. *J. Morphol.* 272, 1153–1169. doi: 10.1002/jmor.10975

Santagata, S., and Zimmer, R. L. (2002). Comparison of the neuromuscular systems among actinotroch larvae: systematic and evolutionary implications. *Evol. Dev.* 4, 43–54. doi: 10.1046/j.1525-142x.2002.01056.x

Scherholz, M., Redl, E., Wollesen, T., Todt, C., and Wanninger, A. (2015). From complex to simple: myogenesis in an aplacophoran mollusk reveals key traits in aculiferan evolution. *BMC Evol. Biol.* 15:201. doi: 10.1186/s12862-015-0467-1

Schindelin, J., Arganda-Carreras, I., Frise, E., Kaynig, V., Longair, M., Pietzsch, T., et al. (2012). Fiji: an open-source platform for biological-image analysis. *Nat. Methods* 9, 676–682. doi: 10.1038/nmeth.2019

Schneider, C. A., Rasband, W. S., and Eliceiri, K. W. (2012). NIH Image to ImageJ: 25 years of image analysis. *Nat. Methods* 9, 671–675. doi: 10.1038/nmeth.2089

Schwartz, M. L. (2009). *Untying a Gordian Knot of Worms: Systematics and Taxonomy of the Pilidiophora (Phylum Nemertea) from Multiple Data Sets*. [Doctor of Philosophy dissertation]. George Washington University, Washington, DC.

Sonnleitner, B., Schwaha, T., and Wanninger, A. (2014). Inter- and intraspecific plasticity in distribution patterns of immunoreactive compounds in actinotroch larvae of Phoronida (Lophotrochozoa). *J. Zool. Syst. Evol. Res.* 52, 1–14. doi: 10.1111/jzs.12043

Stricker, S. A., and Reed, C. G. (1981). Larval morphology of the nemertean *Carcinonemertes epialti* (Nemertea: Hoplonemertea). *J. Morphol.* 169, 61–70. doi: 10.1002/jmor.1051690106

Sun, X., Zheng, Y., Yu, T., Wu, B., Liu, Z., Zhou, L., et al. (2019). Developmental dynamics of myogenesis in Yesso Scallop *Patinopecten yessoensis*. *Comp. Biochem. Physiol. Part B Biochem. Mol. Biol.* 228, 51–60. doi: 10.1016/j.cbpb.2018.11.004

Temereva, E. N. (2012). Ventral nerve cord in *Phoronopsis harmeri* larvae. *J. Exp. Zool. Part B Mol. Dev. Evol.* 318, 26–34. doi: 10.1002/jez.b.21437

Temereva, E. N., and Tsitrin, E. B. (2013). Development, organization, and remodeling of phoronid muscles from embryo to metamorphosis (Lophotrochozoa: Phoronida). *BMC Dev. Biol.* 13:14. doi: 10.1186/1471-213X-13-14

Temereva, E. N., and Tsitrin, E. B. (2014). Development and organization of the larval nervous system in *Phoronopsis harmeri*: new insights into phoronid phylogeny. *Front. Zool.* 11:3. doi: 10.1186/1742-9994-11-3

Temereva, E., and Wanninger, A. (2012). Development of the nervous system in *Phoronopsis harmeri* (Lophotrochozoa, Phoronida) reveals both deuterostome- and trochozoan-like features. *BMC Evol. Biol.* 12:121. doi: 10.1186/1471-2148-12-121

Thollesson, M., and Norenburg, J. L. (2003). Ribbon worm relationships: a phylogeny of the phylum Nemertea. *Proc. Biol. Sci.* 270, 407–415. doi: 10.1098/rspb.2002.2254

von Döhren, J. (2011). The fate of the larval epidermis in the Desor-larva of *Lineus viridis* (Pilidiophora, Nemertea) displays a historically constrained functional shift from planktotrophy to lecithotrophy. *Zoomorphology* 130, 189–196. doi: 10.1007/s00435-011-0131-2

von Döhren, J. (2015). "Nemertea," in *Evolutionary Developmental Biology of Invertebrates Vol. 2: Lophotrochozoa (Spiralia)*, ed. A. Wanninger (Wien: Springer Verlag), 155–192. doi: 10.1007/978-3-7091-1871-9

von Döhren, J. (2016). Development of the nervous system of *Carinina ochracea* (Palaeonemertea, Nemertea). *PLoS One* 11:e0165649. doi: 10.1371/journal.pone.0165649

von Reumont, B. M., Lüddecke, T., Timm, T., Lochnit, G., Vilcinskas, A., von Döhren, J., et al. (2020). Proteo-transcriptomic analysis identifies potential novel toxins secreted by the predatory, prey-piercing ribbon worm *Amphiporus lactifloreus*. *Mar. Drugs* 18:407. doi: 10.3390/MD18080407

Wang, J., Zhang, L., Lian, S., Qin, Z., Zhu, X., Dai, X., et al. (2020). Evolutionary transcriptomics of metazoan biphasic life cycle supports a single intercalation origin of metazoan larvae. *Nat. Ecol. Evol.* 4, 725–736. doi: 10.1038/s41559-020-1138-1

Wanninger, A. (2008). Comparative lophotrochozoan neurogenesis and larval neuroanatomy: recent advances from previously neglected taxa. *Acta Biol. Hung.* 59(Suppl.), 127–136. doi: 10.1556/ABiol.59.2008.Suppl.21

Wanninger, A. (2009). Shaping the things to come: Ontogeny of lophotrochozoan neuromuscular systems and the tetraneuralia concept. *Biol. Bull.* 216, 293–306. doi: 10.1086/BBLv216n3p293

Wanninger, A. (2015). Morphology is dead - long live morphology! Integrating MorphoEvoDevo into molecular EvoDevo and phylogenomics. *Front. Ecol. Evol.* 3:54. doi: 10.3389/fevo.2015.00054

Wanninger, A., and Wollesen, T. (2015). "Mollusca," in *Evolutionary Developmental Biology of Invertebrates Vol. 2: Lophotrochozoa (Spiralia)*, ed. A. Wanninger (Wien: Springer), 1–289. doi: 10.1007/978-3-7091-1871-9

Wanninger, A., Koop, D., and Degnan, B. M. (2005). Immunocytochemistry and metamorphic fate of the larval nervous system of *Triphyllozoon mucronatum* (Ectoprocta: Gymnolaemata: Cheilostomata). *Zoomorphology* 124, 161–170. doi: 10.1007/s00435-005-0004-7

Conflict of Interest: The author declares that the research was conducted in the absence of any commercial or financial relationships that could be construed as a potential conflict of interest.